Galaxy Zoo: evidence for diverse star formation histories through the green valley

R. J. Smethurst,[1][*] C. J. Lintott,[1] B. D. Simmons,[1] K. Schawinski,[2] P. J. Marshall,[1,3] S. Bamford,[4] L. Fortson,[5] S. Kaviraj,[6] K. L. Masters,[7] T. Melvin,[7] R. C. Nichol,[7] R. A. Skibba[8] and K. W. Willett[5]

[1]*Oxford Astrophysics, Department of Physics, University of Oxford, Denys Wilkinson Building, Keble Road, Oxford OX1 3RH, UK*
[2]*Institute for Astronomy, Department of Physics, ETH Zurich, Wolfgang-Pauli Strasse 27, CH-8093 Zurich, Switzerland*
[3]*Kavli Institute for Particle Astrophysics and Cosmology, Stanford University, 452 Lomita Mall, Stanford, CA 95616, USA*
[4]*School of Physics and Astronomy, The University of Nottingham, University Park, Nottingham NG7 2RD, UK*
[5]*School of Physics and Astronomy, University of Minnesota, 116 Church St SE, Minneapolis, MN 55455, USA*
[6]*Centre for Astrophysics Research, University of Hertfordshire, College Lane, Hatfield, Hertfordshire AL10 9AB, UK*
[7]*Institute of Cosmology and Gravitation, University of Portsmouth, Dennis Sciama Building, Barnaby Road, Portsmouth PO1 3FX, UK*
[8]*Center for Astrophysics and Space Sciences, University of California San Diego, 9500 Gilman Drive, La Jolla, CA 92093, USA*

ABSTRACT

Does galaxy evolution proceed through the green valley via multiple pathways or as a single population? Motivated by recent results highlighting radically different evolutionary pathways between early- and late-type galaxies, we present results from a simple Bayesian approach to this problem wherein we model the star formation history (SFH) of a galaxy with two parameters, $[t, \tau]$ and compare the predicted and observed optical and near-ultraviolet colours. We use a novel method to investigate the morphological differences between the most probable SFHs for both disc-like and smooth-like populations of galaxies, by using a sample of 126 316 galaxies ($0.01 < z < 0.25$) with probabilistic estimates of morphology from Galaxy Zoo. We find a clear difference between the quenching time-scales preferred by smooth- and disc-like galaxies, with three possible routes through the green valley dominated by smooth- (rapid time-scales, attributed to major mergers), intermediate- (intermediate time-scales, attributed to minor mergers and galaxy interactions) and disc-like (slow time-scales, attributed to secular evolution) galaxies. We hypothesize that morphological changes occur in systems which have undergone quenching with an exponential time-scale $\tau < 1.5\,\mathrm{Gyr}$, in order for the evolution of galaxies in the green valley to match the ratio of smooth to disc galaxies observed in the red sequence. These rapid time-scales are instrumental in the formation of the red sequence at earlier times; however, we find that galaxies currently passing through the green valley typically do so at intermediate time-scales.[†]

Key words: galaxies: abundances – galaxies: evolution – galaxies: general – galaxies: photometry – galaxies: statistics.

1 INTRODUCTION

Previous large-scale surveys of galaxies have revealed a bimodality in the colour–magnitude diagram (CMD) with two distinct populations; one at relatively low mass, with blue optical colours and another at relatively high mass, with red optical colours (Baldry et al. 2004, 2006; Willmer et al. 2006; Ball, Loveday & Brunner 2008; Brammer et al. 2009). These populations were dubbed the 'blue cloud' and 'red sequence', respectively (Chester & Roberts 1964; Bower, Lucey & Ellis 1992; Driver et al. 2006; Faber et al. 2007). The Galaxy Zoo project (Lintott et al. 2011), which produced morphological classifications for a million galaxies, helped to confirm that this bimodality is not entirely morphology driven (Strateva et al. 2001; Salim et al. 2007; Schawinski et al. 2007; Constantin, Hoyle & Vogeley 2008; Bamford et al. 2009; Skibba et al. 2009), detecting larger fractions of spiral galaxies in the red sequence (Masters et al. 2010) and elliptical galaxies in the blue cloud (Schawinski et al. 2009) than had previously been detected.

The sparsely populated colour space between these two populations, the so-called green valley, provides clues to the nature and duration of galaxies' transitions from blue to red. This transition must occur on rapid time-scales, otherwise there would be an accumulation of galaxies residing in the green valley, rather than an accumulation in the red sequence as is observed (Arnouts et al. 2007; Martin et al. 2007). Green valley galaxies have therefore long been thought of as the 'crossroads' of galaxy evolution, a transition population between the two main galactic stages of the star-forming blue cloud and the 'dead' red sequence (Bell et al. 2004; Faber et al. 2007; Martin et al. 2007; Schiminovich et al. 2007; Wyder et al. 2007; Mendez et al. 2011; Gonçalves et al. 2012; Pan et al. 2014; Schawinski et al. 2014).

The intermediate colours of these green valley galaxies have been interpreted as evidence for recent quenching (suppression) of star formation (Salim et al. 2007). Star-forming galaxies are observed to lie on a well-defined mass–SFR relation; however, quenching a galaxy causes it to depart from this relation (Noeske et al. 2007; Peng et al. 2010; see Fig. 6).

By studying the galaxies which have just left this mass–SFR relation, we can probe the quenching mechanisms by which this occurs. There have been many previous theories for the initial triggers of these quenching mechanisms, including negative feedback from AGN (Di Matteo, Springel & Hernquist 2005; Martin et al. 2007; Nandra et al. 2007; Schawinski et al. 2007), mergers (Darg et al. 2010; Cheung et al. 2012; Barro et al. 2013), supernovae winds (Marasco, Fraternali & Binney 2012), cluster interactions (Coil et al. 2008; Mendez et al. 2011; Fang et al. 2013) and secular evolution (Masters et al. 2010, 2011; Mendez et al. 2011). By investigating the *amount* of quenching that has occurred in the blue cloud, green valley and red sequence; and by comparing the amount across these three populations, we can apply some constraints to these theories.

We have been motivated by a recent result suggesting two contrasting evolutionary pathways through the green valley by different morphological types (Schawinski et al. 2014, hereafter S14), specifically that late-type galaxies quench very slowly and form a nearly static disc population in the green valley, whereas early-type galaxies quench very rapidly, transitioning through the green valley and on to the red sequence in ~1 Gyr (Wong et al. 2012). That study used a toy model to examine quenching across the green valley. Here we implement a novel method utilizing Bayesian statistics (for a comprehensive overview of Bayesian statistics, see either MacKay 2003; Sivia 1996) in order to find the most likely model description of the star formation histories (SFHs) of galaxies in the three populations. This method also enables a direct comparison with our current understanding of galaxy evolution from stellar population synthesis (SPS, see Section 3) models.

Through this approach, we aim to determine the following:

(i) What previous SFH causes a galaxy to reside in the green valley at the current epoch?

(ii) Is the green valley a transitional or static population?

(iii) If the green valley is a transitional population, how many routes through it are there?

(iv) Are there morphology-dependent differences between these routes through the green valley?

This paper proceeds as follows. Section 2 contains a description of the sample data, which is used in the Bayesian analysis of an exponentially declining SFH model, all described in Section 3. Section 4 contains the results produced by this analysis, with Section 5 providing a detailed discussion of the results obtained. We also summarize our findings in Section 6. The zero-points of all *ugriz*

magnitudes are in the AB system and where necessary we adopt the *WMAP* Seven-Year Cosmological parameters (Jarosik et al. 2011) with $(\Omega_m, \Omega_\lambda, h) = (0.26, 0.73, 0.71)$.

2 DATA

2.1 Multiwavelength data

The galaxy sample is compiled from publicly available optical data from the Sloan Digital Sky Survey (SDSS; York et al. 2000) Data Release 8 (Aihara et al. 2011). Near-ultraviolet (NUV) photometry was obtained from the *Galaxy Evolution Explorer* (GALEX; Martin et al. 2005) and was matched with a search radius of 1 arcsec in right ascension and declination.

Observed optical and ultraviolet fluxes are corrected for galactic extinction (Oh et al. 2011) by applying the Cardelli, Clayton & Mathis (1989) law, giving a typical correction of $u - r \sim 0.05$. We also adopt k-corrections to $z = 0.0$ and obtain absolute magnitudes from the NYU-VAGC (Blanton et al. 2005; Padmanabhan et al. 2008; Blanton & Roweis 2007), giving a typical $u - r$ correction of ~0.15 mag. The change in the $u - r$ colour due to both corrections therefore ranges from $\Delta u - r \sim 0.2$ at low redshift, increasing up to $\Delta u - r \sim 1.0$ at $z \sim 0.25$, which is consistent with the expected k-corrections shown in fig. 15 of Blanton & Roweis (2007). These corrections were calculated by Bamford et al. (2009) for the entire Galaxy Zoo sample. These corrections are a crucial aspect of this work since a $\Delta u - r \sim 1.0$ can cause a galaxy to cross the definition between blue cloud, green valley and red sequence.

We obtained star formation rates (SFRs) and stellar masses from the MPA-JHU catalogue (Kauffmann et al. 2003; Brinchmann et al. 2004; average values, AVG, corrected for aperture and extinction), which are in turn calculated from the SDSS spectra and photometry.

We further select a sub-sample with detailed morphological classifications, as described below, to give a volume-limited sample in the redshift range $0.01 < z < 0.25$.

2.2 Galaxy Zoo 2 Morphological classifications

In this investigation, we use visual classifications of galaxy morphologies from the Galaxy Zoo 2[1] (GZ2) citizen science project (Willett et al. 2013), which obtains multiple independent classifications for each galaxy image; the full question tree for each image is shown in fig. 1 of Willett et al. (2013).

The GZ2 project consists of 304 022 images from the SDSS DR8 (a subset of those classified in Galaxy Zoo 1; GZ1) all classified by *at least* 17 independent users, with the mean number of classifications standing at ~42. The GZ2 sample is more robust than the GZ1 sample and provides more detailed morphological classifications, including features such as bars, the number of spiral arms and the ellipticity of smooth galaxies. It is for these reasons we use the GZ2 sample, as opposed to the GZ1, allowing for further investigation of specific galaxy classes in the future (see Section 5.4). The only selection that was made on the sample was to remove objects considered to be stars, artefacts or merging pairs by the users (i.e. with $p_{star/artefact} \geq 0.8$ or $p_{merger} \geq 0.420$; see table 3 in Willett et al. 2013 and discussion for details of this fractional limit). Further to this, we required NUV photometry from the *GALEX* survey, within which ~42 per cent of the GZ2 sample were observed, giving a total sample size of 126 316 galaxies. The completeness of this sub-sample
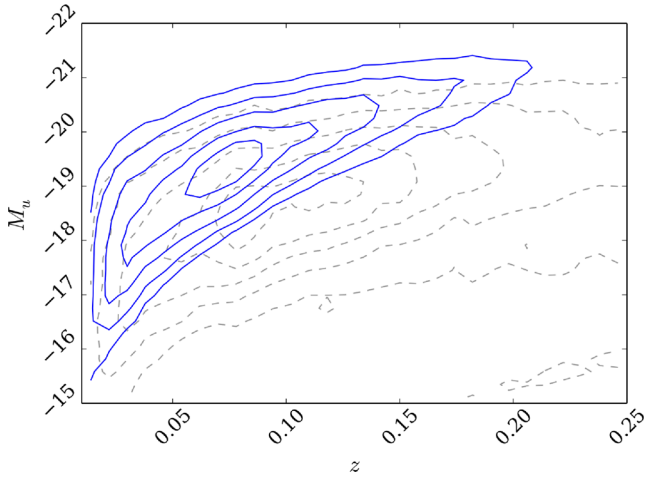
---

[1] http://zoo2.galaxyzoo.org/

Figure 1. Absolute *u*-band magnitude against redshift for the whole of SDSS (grey dashed lines) in comparison to the GZ2 sub-sample (blue solid lines). Typical Milky Way L_* galaxies with $M_u \sim -20.5$ are still included in the GZ2 sub-sample out to the highest redshift of $z \sim 0.25$.

of GZ2 matched to *GALEX* is shown in Fig. 1 with the *u*-band absolute magnitude against redshift for this sample compared with the SDSS data set. Typical Milky Way L_* galaxies with $M_u \sim -20.5$ are still included in the GZ2 sub-sample out to the highest redshift of $z \sim 0.25$; however dwarf and lower mass galaxies are only detected at the lowest redshifts.

The first task of GZ2 asks users to choose whether a galaxy is mostly smooth, is featured and/or has a disc or is a star/artefact. Unlike other tasks further down the decision tree, every user who classifies a galaxy image will complete this task (others, such as whether the galaxy has a bar, is dependent on a user having first classified it as a featured galaxy). Therefore, we have the most statistically robust classifications at this level.

The classifications from users produces a vote fraction for each galaxy (the debiased fractions calculated by Willett et al. (2013) were used in this investigation); for example if 80 of 100 people thought a galaxy was disc shaped, whereas 20 out of 100 people thought the same galaxy was smooth in shape (i.e. elliptical), that galaxy would have vote fractions $p_s = 0.2$ and $p_d = 0.8$. In this example this galaxy would be included in the *'clean'* disc sample

($p_d \geq 0.8$) according to Willett et al. (2013) and would be considered a late-type galaxy. All previous Galaxy Zoo projects have incorporated extensive analysis of volunteer classifications to measure classification accuracy and bias, and compute user weightings (for a detailed description of debiasing and consistency-based user weightings, see either section 3 of Lintott et al. 2008 or section 3 of Willett et al. 2013).

The classifications are highly accurate and provide a continuous scale of morphological features, as shown in Fig. 2, rather than a simple binary classification separating elliptical and disc galaxies. These classifications allow each galaxy to be considered as a probabilistic object with both bulge and disc components. For the first time, we incorporate this advantage of the GZ classifications into a large statistical analysis of how elliptical and disc galaxies differ in their SFHs.

2.3 Defining the green valley

To define which of the sample of 126 316 galaxies were in the green valley, we looked to previous definitions in the literature defining the separation between the red sequence and blue cloud to ensure comparisons can be made with other works. Baldry et al. (2004) used a large sample of local galaxies from the SDSS to trace this bimodality by fitting double Gaussians to the CMD without cuts in morphology. Their relation is defined in their equation (11) as

$$C'_{ur}(M_r) = 2.06 - 0.244 \tanh\left(\frac{M_r + 20.07}{1.09}\right) \quad (1)$$

and is shown in Fig. 3 by the dashed line in comparison to both the GZ2 sub-sample (left) and the SDSS data from Baldry et al. (2004). This ensures that the definition of the green valley used is derived from a complete sample, rather than from our sample that is dominated by blue galaxies due to the necessity for NUV photometry. Any galaxy within $\pm 1\sigma$ of this relationship, shown by the solid lines in Fig. 3, is therefore considered a green valley galaxy. The decomposition of the sample into red sequence, green valley and blue cloud galaxies is shown in Table 1 along with further sub-sections by galaxy type. This table also lists the definitions we adopt henceforth for early-type ($p_s \geq 0.8$), late-type ($p_d \geq 0.8$), smooth-like ($p_s > 0.5$) and disc-like ($p_d > 0.5$) galaxies.
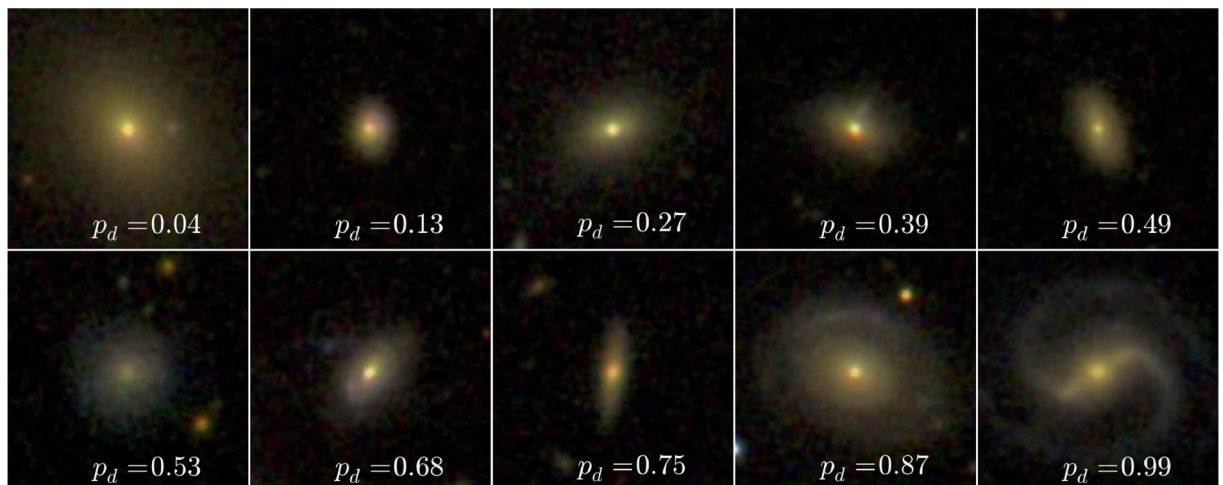

Figure 2. Randomly selected SDSS *gri* composite images showing the continuous probabilistic nature of the Galaxy Zoo sample from a redshift range $0.070 < z < 0.075$. The debiased disc vote fraction (see Willett et al. 2013) for each galaxy is shown. The scale for each image is 0.099 arcsec pixel^{-1}.
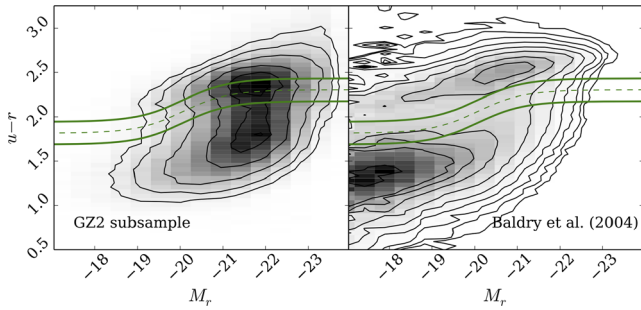
Figure 3. CMD for the GZ2 sub-sample (left) and the SDSS sample from Baldry et al. (2004) with the definition between the blue cloud and the red sequence from Baldry et al. (2004) with the dashed line, as defined in equation (1). The solid lines show $\pm 1\sigma$ either side of this definition; any galaxy within the boundary of these two solid lines is considered a green valley galaxy. The lack of red sequence galaxies due to the necessity for NUV *GALEX* colours skews the apparent location of the green valley; therefore, a literature definition of the green valley is used to ensure comparisons can be made with other works.

3 MODELS

In the following section, the quenched SFH models are described in Section 3.1 and the probabilistic fitting method to the data is described in Section 3.2.

3.1 Quenching models

The quenched SFH of a galaxy can be simply modelled as an exponentially declining SFR across cosmic time ($0 \le t$ [Gyr] $\le$ 13.8) as

$$\text{SFR} = \begin{cases} i_{\text{sfr}}(t_q) & \text{if } t < t_q \\ i_{\text{sfr}}(t_q) \times \exp\left(\frac{-(t-t_q)}{\tau}\right) & \text{if } t > t_q, \end{cases} \quad (2)$$

where t_q is the onset time of quenching, τ is the time-scale over which the quenching occurs and i_{sfr} is an initial constant SFR dependent on t_q. A smaller τ value corresponds to a rapid quench, whereas a larger τ value corresponds to a slower quench.

We assume that all galaxies formed at a time $t = 0\,\text{Gyr}$ with an initial burst of star formation. The mass of this initial burst is controlled by the value of the i_{sfr} which is set as the average specific SFR (sSFR) at the time of quenching t_q. Peng et al. (2010) defined a relation (their equation 1) between the average sSFR and redshift (cosmic time, t) by fitting to measurements of the mean sSFR of blue

star-forming galaxies from SDSS, zCOSMOS and literature values at increasing redshifts (Daddi et al. 2007; Elbaz et al. 2007):

$$\text{sSFR}(m, t) = 2.5 \left(\frac{m}{10^{10}\,\text{M}_\odot}\right)^{-0.1} \left(\frac{t}{3.5\,\text{Gyr}}\right)^{-2.2} \text{Gyr}^{-1}. \quad (3)$$

Beyond $z \sim 2$ the characteristic SFR flattens and is roughly constant back to $z \sim 6$. The cause for this change is not well understood but can be seen across similar observational data (González et al. 2010; Peng et al. 2010; Béthermin et al. 2012). Motivated by these observations, the relation defined in Peng et al. (2010) is taken up to a cosmic time of $t = 3\,\text{Gyr}(z \sim 2.3)$ and prior to this a constant average SFR is assumed (see Fig. 7). At the point of quenching, t_q, the models are defined to have an SFR which lies on this relationship for the sSFR, for a galaxy with mass, $m = 10^{10.27}\,\text{M}_\odot$ (the mean mass of the GZ2 sample; see Section 4 and Fig. 7).

Under these assumptions the average SFR of our models will result in a lower value than the relation defined in Peng et al. (2010) at all cosmic times; each galaxy only resides on the 'main sequence' at the point of quenching. However, galaxies cannot remain on the 'main sequence' from early to late times throughout their entire lifetimes given the unphysical stellar masses and SFRs this would result in at the current epoch in the local Universe (Béthermin et al. 2012; Heinis et al. 2014). If we were to include prescriptions for no quenching, starbursts, mergers, AGN, etc., into our models we would improve on our reproduction of the average SFR across cosmic time; however, we chose to initially focus on the simplest model possible.

Once this evolutionary SFR is obtained, it is convolved with the Bruzual & Charlot (2003) population synthesis models to generate a model SED at each time step. The observed features of galaxy spectra can be modelled using simple stellar population techniques which sum the contributions of individual, coeval, equal-metallicity stars. The accuracy of these predictions depends on the completeness of the input stellar physics. Comprehensive knowledge is therefore required of (i) stellar evolutionary tracks and (ii) the initial mass function (IMF) to synthesize a stellar population accurately.

These SPS models are an extremely well explored (and often debated) area of astrophysics (Maraston 2005; Eminian et al. 2008; Conroy, Gunn & White 2009; Falkenberg, Kotulla & Fritze 2009; Chen et al. 2010; Kriek et al. 2010; Miller, Rose & Cecil 2011; Melbourne et al. 2012). In this investigation, we chose to utilize the Bruzual & Charlot (2003) *GALEXEV* SPS models, to allow a direct comparison with S14, along with a Chabrier (2003) IMF, across a large wavelength range ($0.0091 < \lambda\,[\mu\text{m}] < 160$) with solar metal-lically (m62 in the Bruzual & Charlot 2003 models, hereafter BC03).

Fluxes from stars younger than 3Myr in the SPS model are suppressed to mimic the large optical depth of protostars embedded in

Table 1. The decomposition of the GZ2 sample by galaxy type into the subsets of the CMD.

	All	Red sequence	Green valley	Blue cloud
Smooth-like ($p_s > 0.5$)	42 453	17 424	10 687	14 342
	(33.6 per cent)	(61.9 per cent)	(44.6 per cent)	(19.3 per cent)
Disc-like ($p_d > 0.5$)	83 863	10 722	13 257	59 884
	(80.7 per cent)	(38.1 per cent)	(55.4 per cent)	(47.4 per cent)
Early-type ($p_s \ge 0.8$)	10 517	5337	2496	2684
	(8.3 per cent)	(18.9 per cent)	(10.4 per cent)	(3.6 per cent)
Late-type ($p_s \ge 0.8$)	51 470	4493	6817	40 430
	(40.9 per cent)	(15.9 per cent)	(28.5 per cent)	(54.4 per cent)
Total	**126 316**	28 146	23 944	74 226
	(100.0 per cent)	(22.3 per cent)	(18.9 per cent)	(58.7 per cent)

dusty formation cloud (as in S14), then filter transmission curves are applied to the fluxes to obtain AB magnitudes and therefore colours. For a particular galaxy at an observed redshift, z, we define the observed time, t^{obs} for that galaxy using the standard cosmological conversion between redshift and time. We utilize the SFH models at this observed time for each individual galaxy to compare the predicted model and observed colours directly.

Fig. 4 shows these predicted optical and NUV colours at a time of $t^{\mathrm{obs}} = 12.8$ Gyr (the average observed time of the GZ2 sample, $z \sim 0.076$) provided by the exponential SFH model. These predicted colours will be referred to as $d_{c,\mathrm{p}}(t_q, \tau, t^{\mathrm{obs}})$, where c = {opt,NUV} and p = predicted. The SFR at a time of $t^{\mathrm{obs}} = 12.8$ Gyr is also shown in Fig. 4 to compare how this correlates with the predicted colours. The $u - r$ predicted colour shows an immediate correlation with the SFR, however the NUV $- u$ colour is more sensitive to the value of τ and so is ideal for tracing any recent star formation in a population. At small τ (rapid-quenching time-scales) the NUV $- u$ colour is insensitive to t_q, whereas at large τ (slow quenching time-scales) the colour is very sensitive to t_q. Together the two colours are ideal for tracing the effects of t_q and τ in a population.

We stress here that this model is not a fully hydrodynamical simulation, it is a simple model built in order to test the understanding of the evolution of galaxy populations. These models are therefore not expected to accurately determine the SFH of every galaxy in the GZ2 sample, in particular galaxies which have not undergone any quenching. In this case the models described above can only attribute a constant SFR to these unquenched galaxies. In reality, there are many possible forms of SFH that a galaxy can take, a few of which have been investigated in previous literature; starbursts (Canalizo & Stockton 2001), a power law (Glazebrook et al. 2003), single stellar populations (Trager et al. 2000; Sánchez-Blázquez et al. 2006; Vazdekis et al. 2010) and metallicity enrichment (de Lucia 2014). Incorporating these different SFHs along with prescriptions for mergers and a reinvigoration of star formation post quench into our models is a possible future extension to this work once the results of this initial study are well enough understood to permit additional complexity to be added.

3.2 Probabilistic fitting

In order to achieve robust conclusions, we conduct a Bayesian analysis (Sivia 1996; MacKay 2003) of our SFH models in comparison to the observed GZ2 sample data. This approach requires consideration of all possible combinations of $\theta \equiv (t_q, \tau)$. Assuming that all galaxies formed at $t = 0$ Gyr with an initial burst of star formation, we can assume that the 'age' of each galaxy in the GZ2 sample is equivalent to an observed time, t_k^{obs} (see Section 2.2). We then use this 'age' to calculate the predicted model colours at this cosmic time for a given combination of θ: $d_{c,\mathrm{p}}(\theta_k, t_k^{\mathrm{obs}})$ for both optical and NUV (c = opt, NUV) colours. We can now directly compare our model colours with the observed GZ2 galaxy colours, so that for a single galaxy k with optical $(u - r)$ colour, $d_{\mathrm{opt},k}$ and NUV (NUV $- u$) colour, $d_{\mathrm{NUV},k}$, the likelihood $P(d_k|\theta_k, t_k^{\mathrm{obs}})$ is

$$P\left(d_k|\theta_k, t_k^{\mathrm{obs}}\right) = \frac{1}{\sqrt{2\pi\sigma_{\mathrm{opt},k}^2}} \frac{1}{\sqrt{2\pi\sigma_{\mathrm{NUV},k}^2}}$$
$$\times \exp\left[-\frac{(d_{\mathrm{opt},k} - d_{\mathrm{opt},p}(\theta_k, t_k^{\mathrm{obs}}))^2}{\sigma_{\mathrm{opt},k}^2}\right]$$
$$\times \exp\left[-\frac{(d_{\mathrm{NUV},k} - d_{\mathrm{NUV},p}(\theta_k, t_k^{\mathrm{obs}}))^2}{\sigma_{\mathrm{NUV},k}^2}\right]. \quad (4)$$
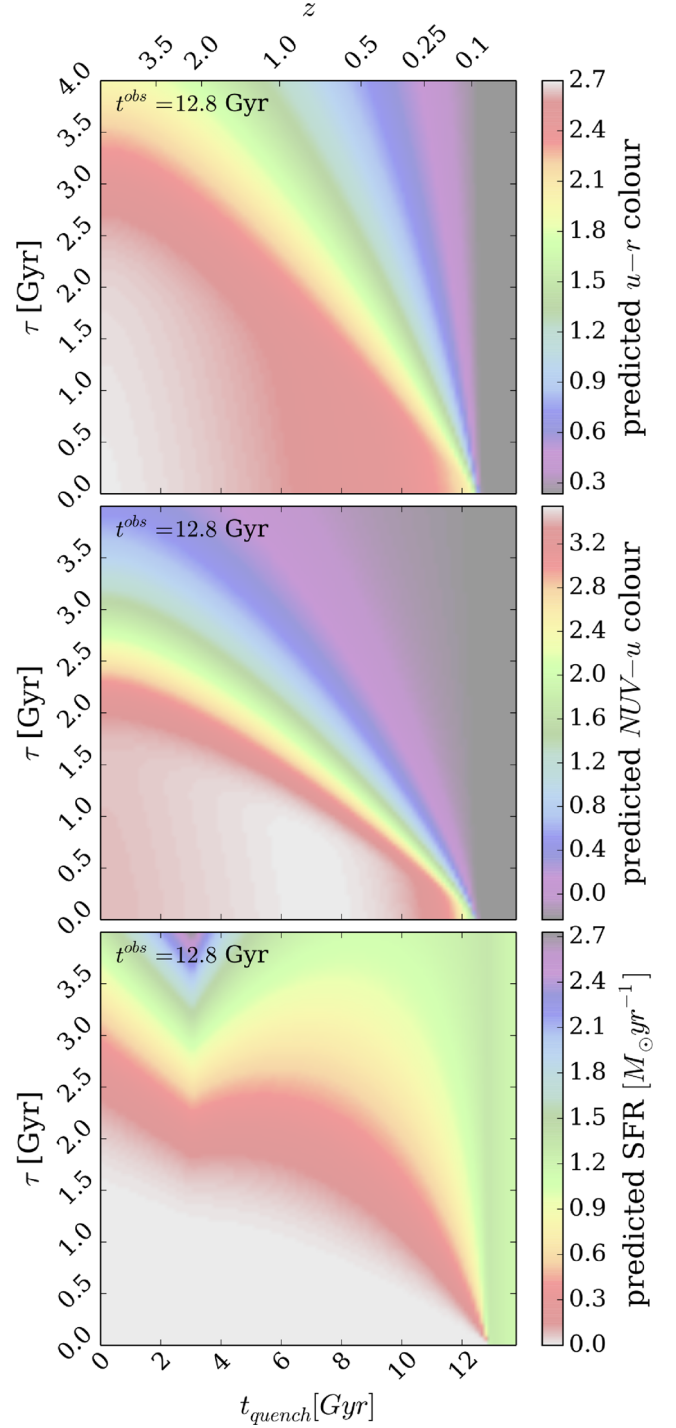

Figure 4. Quenching time-scale τ versus quenching onset time t in all three panels for the quenched SFH models used in STARPY. Colour shadings show model predictions of the $u - r$ optical colour (top panel), NUV $- u$ colour (middle panel), and SFR in $M_\odot \mathrm{yr}^{-1}$ (lower panel), at $t^{\mathrm{obs}} = 12.8$ Gyr, the mean observed redshift of the GZ2 sample (see Section 3.1). The combination of optical and NUV colours is a sensitive measure of the $\theta = [t_q, \tau]$ parameter space. Note that all models with $t > 12.8$ Gyr are effectively unquenched. The 'kink' in the bottom panel is due to the assumption that the sSFR is constant prior to $t \sim 3$ Gyr ($z \sim 2.2$).

We have assumed that $P(d_{opt}|\theta_k, t_k^{obs})$ and $P(d_{NUV}|\theta_k, t_k^{obs})$ are independent of each other and that the errors on the observed colours are also independent. To obtain the probability of each combination of θ values *given* the GZ2 data: $P(\theta_k|d_k, t^{obs})$, i.e. how likely is a single SFH model given the observed colours of a single GZ2 galaxy, we utilize Bayes' theorem:

$$P(\theta_k|d_k, t^{obs}) = \frac{P(d_k|\theta_k, t^{obs})P(\theta_k)}{\int P(d_k|\theta_k, t^{obs})P(\theta_k)d\theta_k}. \quad (5)$$

We assume a flat prior on the model parameters so that

$$P(\theta_k) = \begin{cases} 1 & \text{if } 0 \le t_q \text{ [Gyr]} \le 13.8 \quad \text{and} \quad 0 \le \tau \text{ [Gyr]} \le 4 \\ 0 & \text{otherwise.} \end{cases} \quad (6)$$

As the denominator of equation (5) is a normalization factor, comparison between likelihoods for two different SFH models (i.e. two different combinations of $\theta_k = [t_q, \tau]$) is equivalent to a comparison of the numerators. Calculation of $P(\theta_k|d_k, t^{obs})$ for any θ is possible given galaxy data from the GZ2 sample. Markov Chain Monte Carlo (MCMC; Goodman & Weare 2010; MacKay 2003; Foreman-Mackey et al. 2013) provides a robust comparison of the likelihoods between θ values; here we choose EMCEE,[2] a PYTHON implementation of an affine invariant ensemble sampler by Foreman-Mackey et al. (2013).

This method allows for a more efficient exploration of the parameter space by avoiding those areas with low likelihood. A large number of 'walkers' are started at an initial position where the likelihood is calculated; from there they individually 'jump' to a new area of parameter space. If the likelihood in this new area is greater (less) than the original position then the 'walkers' accept (reject) this change in position. Any new position then influences the direction of the 'jumps' of other walkers. This is repeated for the defined number of steps after an initial 'burn-in' phase. EMCEE returns the positions of these 'walkers', which are analogous to the regions of high probability in the model parameter space. The model outlined above has been coded using the PYTHON programming language into a package named STARPY which has been made freely available for download.[3] An example output from this PYTHON package for a single galaxy from the GZ2 sample in the red sequence is shown in Fig. 5. The contours show the positions of the 'walkers' in the Markov Chain which are analogous to the areas of high probability.

We wish to consider the model parameters for the populations of galaxies across the CMD for both smooth and disc galaxies; therefore, we run the STARPY package on each galaxy in the GZ2 sample. This was extremely time consuming; for each combination of θ values which EMCEE proposes, a new SFH must be built, prior to convolving it with the BC03 SPS models at the observed age and then predicted colours calculated from the resultant SED. For a single galaxy this takes up to 2 h on a typical desktop machine for long Markov Chains. A look-up table was therefore generated at $50t^{obs}$, for $100t_{quench}$ and 100τ values; this was then interpolated over for a given observed galaxy's age and proposed θ values at each step in the Markov Chain. This ensures that a single galaxy takes approximately 2 min to run on a typical desktop machine. This interpolation was found to incorporate an error of ± 0.04 into the median θ values found (the 50th percentile position of the walkers; see Appendix B for further information).

Using this look-up table, each of the 126 316 total galaxies in the GZ2 sample was run through STARPY on multiple cores of a computer
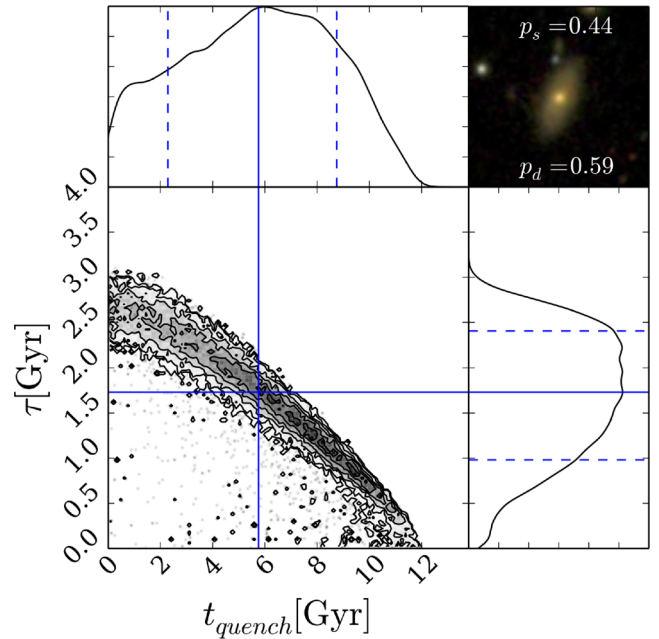
Figure 5. Example output from STARPY for a galaxy within the red sequence. The contours show the positions of the 'walkers' in the Markov Chain (which are analogous to the areas of high probability) for the quenching models described by $\theta = [t_q, \tau]$ and the histograms show the 1D projection along each axis. Solid (dashed) blue lines show the best-fitting model (with $\pm 1\sigma$) to the galaxy data. The postage stamp image from SDSS is shown in the top right along with the debiased vote fractions for smooth (p_s) and disc (p_d) from GZ2.

cluster to obtain the Markov Chain positions (analogous to $P(\theta_k|d_k)$) for each galaxy, k (see Fig. 5). In each case the Markov Chain consisted of 100 'walkers' which took 400 steps in the 'burn-in' phase and 400 steps thereafter, at which point the MCMC acceptance fraction was checked to be within the range $0.25 < f_{acc} < 0.5$ (which was true in all cases). Due to the Bayesian nature of this method, a statistical test on the results is not possible; the output is probabilistic in nature across the entirety of the parameter space.

These individual galaxy positions are then combined to visualize the areas of high probability in the model parameter space across a given population (e.g. the green valley). We do this by first discarding positions with a corresponding probability of $P(\theta_k|d_k) < 0.2$ in order to exclude galaxies which are not well fitted by the quenching model; for example blue cloud galaxies which are still star forming will be poorly fit by a quenching model (see Section 3.1). Using this constraint, 2.4, 7.0 and 5.4 per cent of green, red and blue galaxies, respectively, had *all* of their walker positions discarded. These are not significant enough fractions to affect the results (see Appendix C for more information.) The Markov Chain positions are then binned and weighted by their corresponding logarithmic posterior probability log $[P(\theta_k|d_k)]$, provided by the EMCEE package, to further emphasize the features and differences between each population in the visualization. The GZ2 data also provide uniquely powerful continuous measurements of a galaxy's morphology; therefore, we utilize the user vote fractions to obtain separate model parameter distributions for both smooth and disc galaxies. This is obtained by also weighting by the morphology vote fraction when the binned positions are summed. We stress that this portion of the methodology is a non-Bayesian visualization of the combined individual galaxy results for each population.
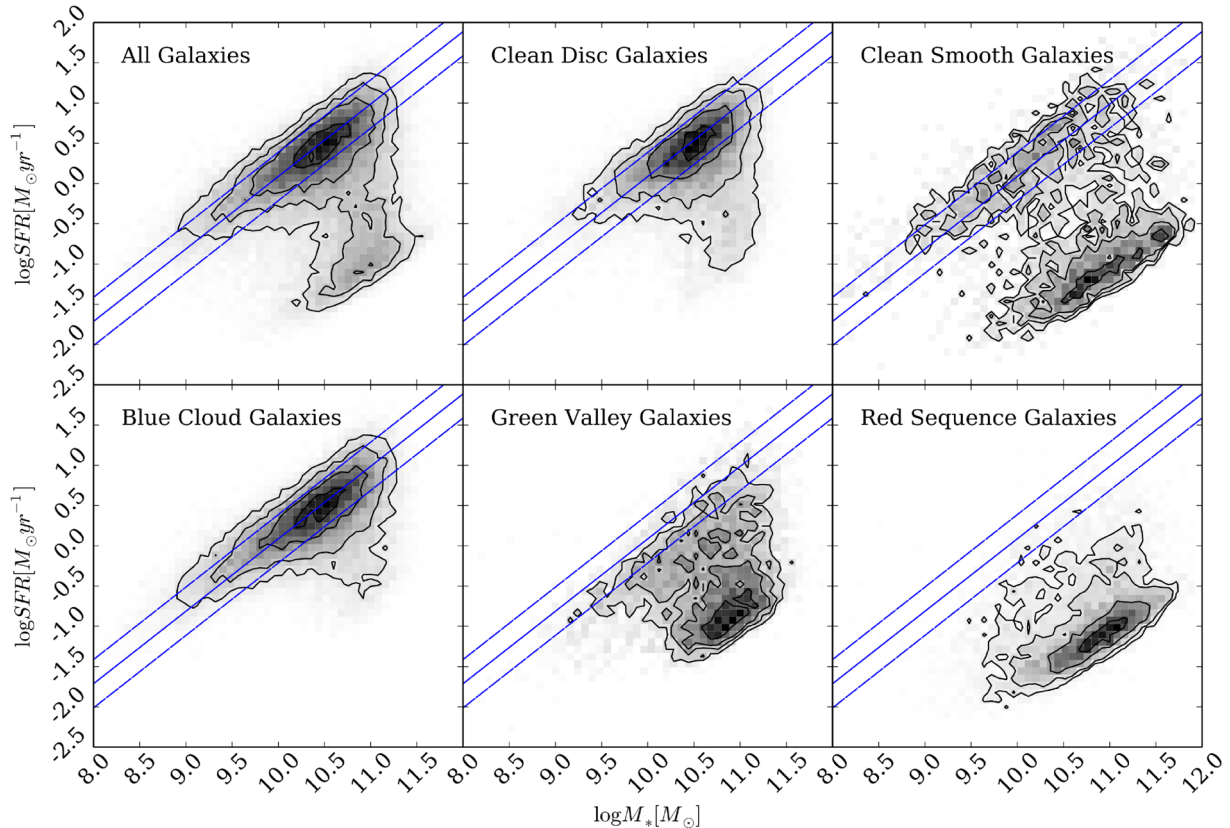
Figure 6. SFR versus stellar mass diagrams show the different populations of galaxies (top row, left to right: all galaxies, GZ2 'clean' disc and smooth galaxies; bottom row, left to right: blue cloud, green valley and red sequence galaxies) and how they contribute to the star-forming sequence (from Peng et al. (2010), shown by the solid blue line with 0.3 dex scatter by the dashed lines). Based on positions in these diagrams, the green valley does appear to be a transitional population between the blue cloud and the red sequence. Detailed analysis of SFHs can elucidate the nature of the different populations' pathways through the green valley. The clean smooth and disc samples are described in Section 2.2.

For example, the galaxy shown in Fig. 5 would contribute almost evenly to both the smooth and disc parameters due to the GZ2 vote fractions. Since galaxies with similar vote fractions contain both a bulge and disc component, this method is effective in incorporating intermediate galaxies which are thought to be crucial to the morphological changes between early- and late-type galaxies. It was the consideration of these intermediate galaxies which was excluded from the investigation by S14.

4 RESULTS

4.1 Initial results

Fig. 6 shows the SFR versus the stellar mass for the observed GZ2 sample which has been split into blue cloud, green valley and red sequence populations as well as into the 'clean' disc and smooth galaxy samples (with GZ2 vote fractions of $p_d \geq 0.8$ and $p_s \geq 0.8$, respectively). The green valley galaxies are indeed a population which have either left, or begun to leave, the star-forming sequence or have some residual star formation still occurring.

The left-hand panel in Fig. 7 shows a handful of quenching models and how they reproduce the observed relationship between the SFR and the mass of a galaxy, including how at the time of quenching they reside on the star-forming sequence shown by the solid black line for a galaxy of mass, $M = 10^{10.27}$ M$_\odot$. The right-hand panel shows how these SFRs translate into the optical–NUV colour–colour plane to reproduce observed colours of green valley

and red sequence galaxies. Some of the SFHs produce colours redder than the apparent peak of the red sequence in the GZ2 subsample; however, this is not the *true* peak of the red sequence due to the necessity for NUV colours from *GALEX* (see Section 2.2).

The majority of the red galaxies in the sample therefore lie towards the *blue end* of the red sequence and have a small amount of residual star formation in order to be detected in the NUV resulting in a specific subset of the red sequence studied in this investigation. Only 47 per cent of the red sequence galaxies present in the entire GZ2 sample are matched with *GALEX* to produce our final sample of 126 316 galaxies, as opposed to 72 per cent of the blue cloud and 53 per cent of the green valley galaxies. This limitation should be taken into account when considering the results in the following sections.

The SFH models were implemented with the STARPY package to produce Figs 8–10 for the red sequence, green valley and blue cloud populations of smooth and disc galaxies, respectively. The percentages shown in Figs 8–10 are calculated as the fractions of the combined posterior probability distribution located in each region of parameter space for a given population.

Since the sample contains such a large number of galaxies, we interpret these fractions as broadly equivalent to the percentage of galaxies in a given population undergoing quenching within the stated time-scale range. Although this is not quantitatively exact, it is nevertheless a useful framework for interpreting the results of combining the individual posterior probability distributions of each galaxy.
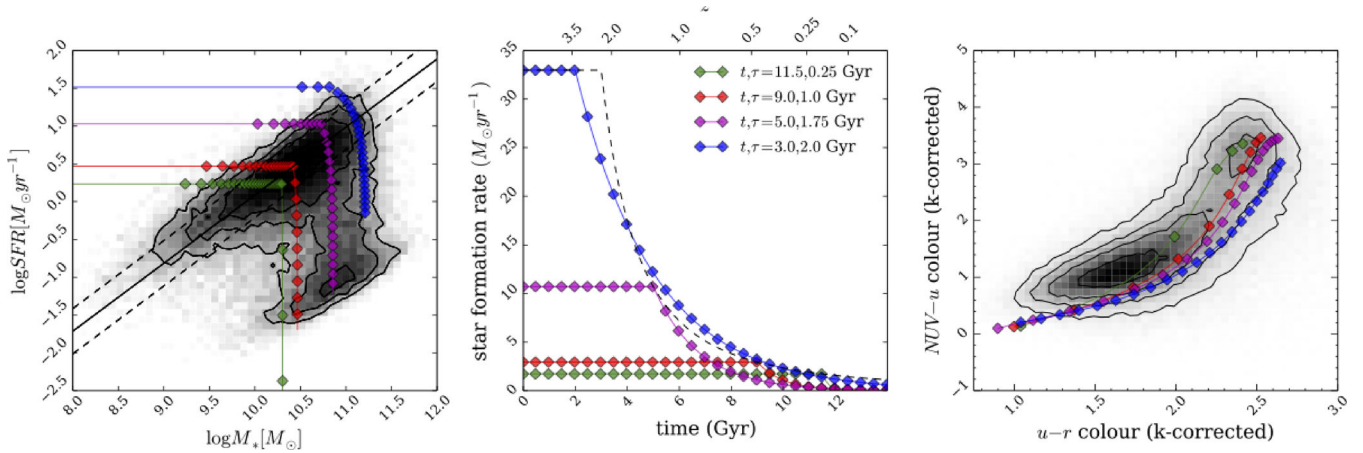
Figure 7. Left-hand panel: SFR versus M_* for all 126 316 galaxies in our full sample (shaded contours), with model galaxy trajectories shown as coloured points/lines with each point representing a time step of 0.5 Gyr. The SFHs of the models are shown in the middle panel, where the SFR is initially constant before quenching at time t and thereafter exponentially declining with a characteristic time-scale τ. We set the SFR at the point of quenching to be consistent with the typical SFR of a star-forming galaxy at the quenching time, t (dashed line; Peng et al. 2010). The full range of models reproduces the observed colour–colour properties of the sample (right-hand panel); for clarity the figures show only four of the possible models explored in this study. Note that some of the model tracks produce colours redder than the apparent peak of the red sequence in the GZ2 sub-sample; however, this is not the true peak of the red sequence due to the necessity for NUV colours from *GALEX* (see Section 2.2).
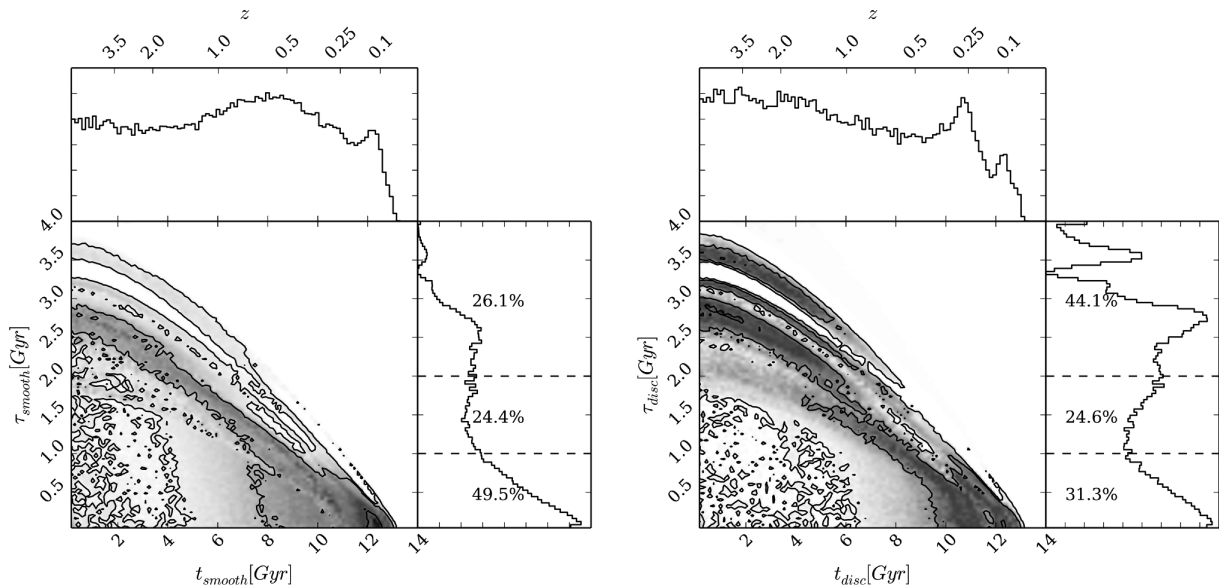
Figure 8. Contour plots showing the combined positions in the Markov Chain for all red galaxies in this study, weighted by the logarithmic probability of each position (see Section 3.2) and also by the morphological vote fractions from GZ2 to give the areas of high probability in the model parameter space for both bulge (left) and disc (right) dominated systems. The histograms show the projection into one dimension for each parameter. The dashed lines show the separation between rapid (τ [Gyr] < 1.0), intermediate (1.0 < τ [Gyr] < 2.0) and slow (τ [Gyr] > 2.0) quenching time-scales with the fraction of the combined posterior probability distribution in each region shown (see Section 3.2).

Also shown in Fig. 11 are the median walker positions (the 50th percentile of the Bayesian probability distribution) of each individual galaxy, split into red, green and blue populations also with a hard cut in the vote fraction of $p_d > 0.5$ and $p_s > 0.5$ to show the disc and smooth populations, respectively. These positions were calculated without discarding any walker positions due to low probability and without weighting by vote fractions; therefore this may be more intuitive to understand than Figs 8–10.

Although the quenching time-scales are continuous in nature, in this section we refer to rapid-, intermediate- and slow-quenching time-scales which correspond to ranges of τ [Gyr] < 1.0, 1.0 <

τ [Gyr] < 2.0 and τ [Gyr] > 2.0, respectively, for ease of discussion.

4.2 The red sample

The left-hand panel of Fig. 8 reveals that smooth galaxies with red optical colours show a preference (49.5 per cent; see Fig. 8) for rapid-quenching time-scales across all cosmic time resulting in a very low current SFR. For these smooth red galaxies we see, at early times only, a preference for slow and intermediate time-scales in the left-hand panel of Fig. 8. Perhaps this is the influence of intermediate
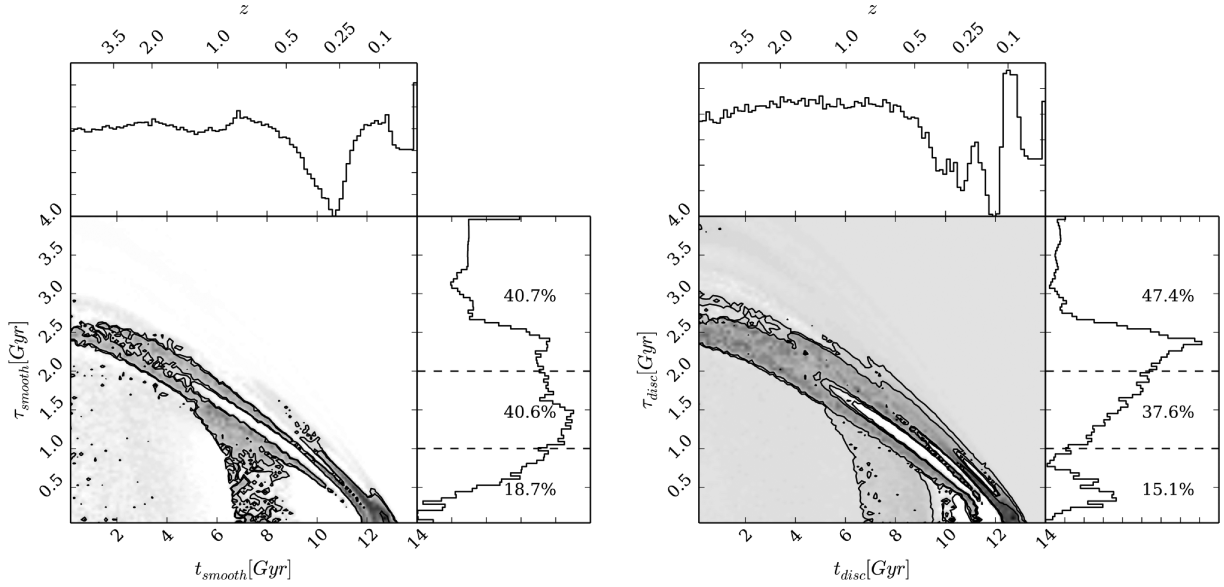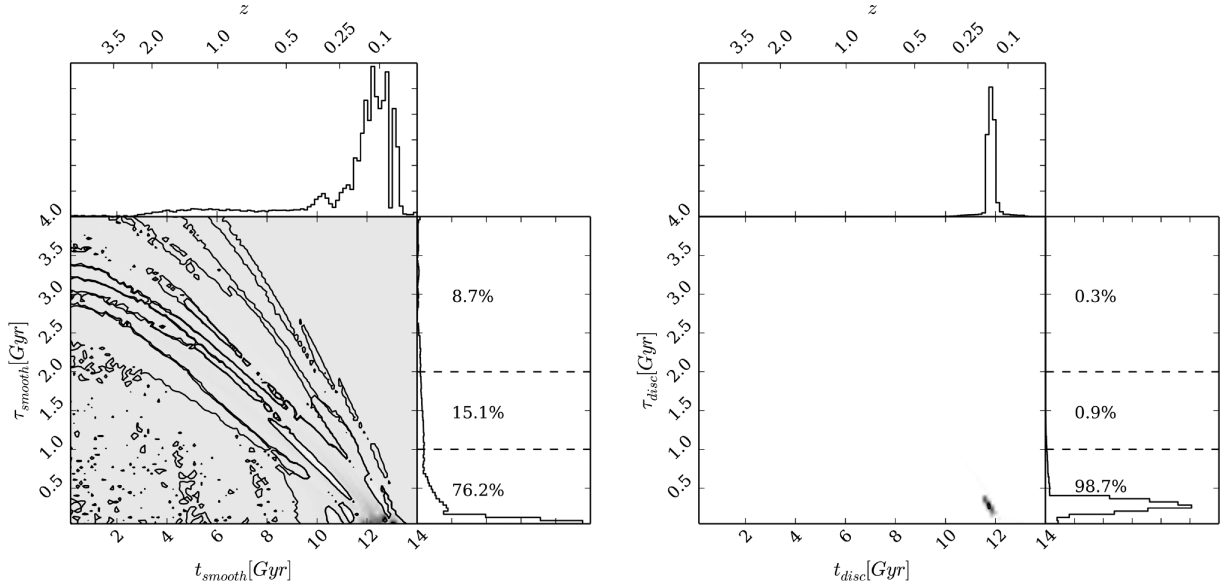
Figure 9. Contour plots showing the combined positions in the Markov Chain for galaxies in the green valley, weighted by the logarithmic probability of each position (see Section 3.2) and also by the morphological vote fractions from GZ2 to give the areas of high probability in the model parameter space for both bulge (left) and disc (right) dominated systems. The histograms show the projection into one dimension for each parameter. The dashed lines show the separation between rapid (τ [Gyr] < 1.0), intermediate ($1.0 < \tau$ [Gyr] < 2.0) and slow (τ [Gyr] > 2.0) quenching time-scales with the fraction of the combined posterior probability distribution in each region shown (see Section 3.2).

Figure 10. Contour plots showing the combined positions in the Markov Chain for galaxies in the blue cloud, weighted by the logarithmic probability of each position (see Section 3.2) and also by the morphological vote fractions from GZ2 to give the areas of high probability in the model parameter space for both bulge (left) and disc (right) dominated systems. The histograms show the projection into one dimension for each parameter. The dashed lines show the separation between rapid (τ [Gyr] < 1.0), intermediate ($1.0 < \tau$ [Gyr] < 2.0) and slow (τ [Gyr] > 2.0) quenching time-scales with the fraction of the combined posterior probability distribution in each region shown (see Section 3.2). Positions with probabilities less than 0.2 are discarded as poorly fit models; therefore, we can conclude unsurprisingly that blue cloud galaxies are not well described by a quenching star formation model.

galaxies (with $p_s \sim p_d \sim 0.5$), hence why similar high-probability areas exist for both the smooth-like and disc-like galaxies in the left- and right-hand panels of Fig. 8. This is especially apparent considering there are far more of these intermediate galaxies than those that are definitively early- or late-types (see Table 1). These galaxies are those whose morphology cannot be easily distinguished either because they are at a large distance or because they are an S0 galaxy whose morphology can be interpreted by different users in

different ways. Willett et al. (2013) find that S0 galaxies expertly classified by Nair & Abraham (2010) are more commonly classified as ellipticals by GZ2 users, but have a significant tail to high disc vote fractions, giving a possible explanation as to the origin of this area of probability.

The right-hand panel of Fig. 8 reveals that red disc galaxies show similar preferences for rapid (31.3 per cent) and slow (44.1 per cent) quenching time-scales. The preference for *very* slow ($\tau > 3.0$ Gyr)
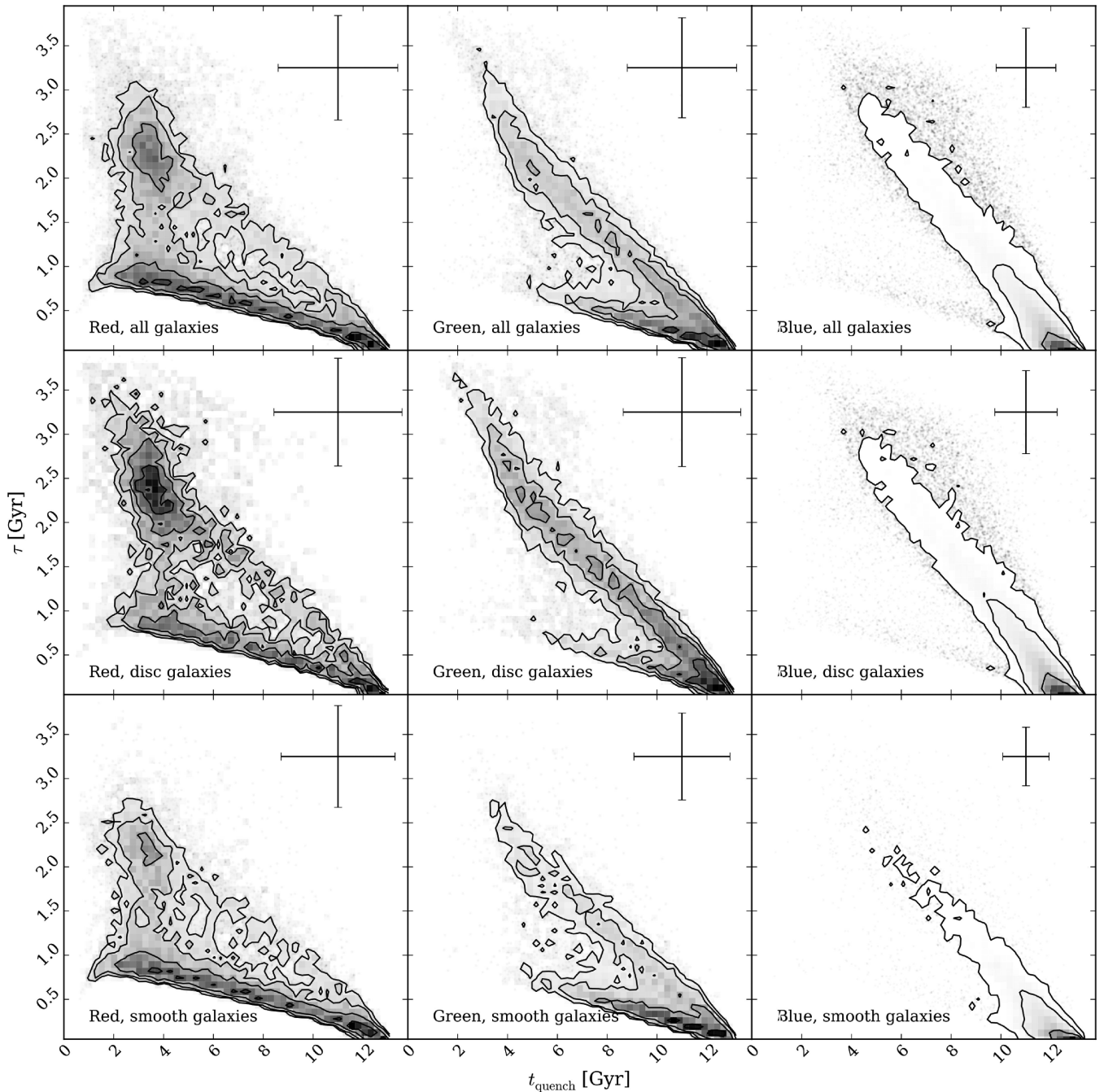
Figure 11. Contours showing the positions in the $[t, \tau]$ parameter space of the median walker position (the 50th percentile; as shown by the intersection of the solid blue lines in Fig. 5) for each galaxy for all (top), disc ($p_d > 0.5$; middle), and smooth ($p_s > 0.5$; bottom) red sequence, green valley and blue cloud galaxies in the left-, middle and right-hand panels, respectively. The error bars on each panel shows the average 68 per cent confidence on the median positions (calculated from the 16th and 84th percentile, as shown by the blue dashed lines in Fig. 5). These positions were calculated without discarding any walker positions due to low probability and without weighting by vote fractions; therefore, this plot may be more intuitive than Figs 8–10. The differences between the smooth and disc populations and between the red, green and blue populations remain clearly apparent.

quenching time-scales (which are not seen in either the green valley or blue cloud, see Figs 9 and 10) suggests that these galaxies have only just reached the red sequence after a very slow evolution across the CMD. Considering their limited number and our requirement for NUV emission, it is likely that these galaxies are currently on the edge of the red sequence having recently (and finally) moved out of the green valley. Table 1 shows that 3.9 per cent of our sample are red sequence clean disc galaxies, i.e. red late-type spirals. This

is, within uncertainties, in agreement with the findings of Masters et al. (2010), who find ~6 per cent of late-type spirals are red when defined by a cut in the $g - r$ optical colour (rather than with $u - r$ as implemented in this investigation) and are at the 'blue end of the red sequence'.

Despite the dominance of slow-quenching time-scales, the red disc galaxies also show some preference for rapid-quenching time-scales (31.3 per cent), similar to the red smooth galaxies but

with a lower probability. Perhaps these rapid-quenching time-scales can also be attributed to a morphological change, suggesting that the quenching has occurred more rapidly than the morphological change to a bulge-dominated system.

Comparing the resultant SFRs for both the smooth- and disc-like galaxies in Fig. 8 by noticing where the areas of high probability lie with respect to the bottom panel of Fig. 4 (which shows the predicted SFR at an observation time of $t \sim 12.8$ Gyr, the average 'observed' time of the GZ2 population) reveals that red disc galaxies with a preference for slow quenching still have some residual star formation occurring, SFR$\sim$0.105 M$_\odot$ yr^{-1}, whereas the smooth galaxies with a dominant preference for rapid quenching have a resultant SFR$\sim$0.0075 M$_\odot$ yr^{-1}. This is approximately 14 times less than the residual SFR still occurring in the red sequence disc galaxies. Within error, this is in agreement with the findings of Tojeiro et al. (2013) who, by using the VErsatile SPectral Analyses spectral fitting code (VESPA; Tojeiro et al. 2007), found that red late-type spirals show 17 times more recent star formation than red elliptical galaxies.

These results for the red galaxies investigated here with NUV emission have many implications for green valley galaxies, as all of these systems must have passed through the green valley on their way to the red sequence.

4.3 Green valley galaxies

In Fig. 9, we can make similar comparisons for the green valley galaxies to those discussed previously for the subset of red galaxies studied. For the red galaxies, an argument can be made for two possible tracks across the green valley, shown by the bimodal nature of both distributions in τ with a common area in the intermediate time-scales region where the rapid and slow time-scales peaked distributions intersect. However in the green valley this intermediate-quenching time-scale region becomes more significant (in agreement with the conclusions of Gonçalves et al. 2012), particularly for the smooth-like galaxies (see the left-hand panel of Fig. 9).

The smooth galaxy parameters favour these intermediate-quenching time-scales (40.6 per cent) with some preference for slow quenching at early times ($z > 1$). The preference for rapid quenching of smooth galaxies has dropped by over a half compared to the red galaxies; however, this will be influenced by the observability of galaxies undergoing such a rapid quench which will spend significantly less time in the transitional population of the green valley. Those galaxies with such a rapid decline in star formation will pass so quickly through the green valley they will be detected at a lower number than those galaxies which have stalled in the green valley with intermediate-quenching time-scales; accounting for the observed number of intermediate galaxies which are present in the green valley and the dominance of rapid time-scales detected for red galaxies for both morphologies.

The disc galaxies of the green valley now overwhelmingly prefer slow-quenching time-scales (47.4 per cent) with a similar amount of intermediate quenching compared to the smooth galaxy parameters (37.6 per cent; see Fig. 9). There is still some preference for galaxies with an SFH which results in a high current SFR, suggesting there are also some late-type galaxies that have just progressed from the blue cloud into the green valley.

If we compare Fig. 9 to Fig. 8, we can see quenching has occurred at later (more recent) cosmic times in the green valley at least for red galaxies for both morphological types. Therefore, both morphologies are tracing the evolution of the red sequence, confirming

that the green valley is indeed a transitional population between blue cloud and red sequence regardless of morphology. Currently as we observe the green valley, its main constituents are very slowly evolving disc-like galaxies along with intermediate- and smooth-like galaxies which pass across it with intermediate time-scales within $\sim$1.0−1.5 Gyr.

Given enough time ($t \sim 4$−5 Gyr), the disc galaxies will eventually fully pass through the green valley and make it out to the red sequence (the right-hand panel of Fig. 7 shows galaxies with $\tau > 1.0$ Gyr do not approach the red sequence within 3 Gyr post quench). This is most likely the origin of the 'red spirals'.

If we consider then that the green valley is a transitional population, then we can expect that the ratio of smooth:disc galaxies that is currently observed in the green valley will evolve into the ratio observed for the red galaxies with NUV emission investigated. Table 1 shows the ratio of smooth : disc galaxies in the observed red sequence of the GZ2 sample is 62: 38 whereas in the green valley it is 45: 55. Making the very simple assumptions that this ratio does not change with redshift and that quenching is the only mechanism which causes a morphological transformation, we can infer that 31.2 per cent of the disc-dominated galaxies currently residing in the green valley would have to undergo a morphological change to a bulge-dominated galaxy. We find that the fraction of the probability for green valley disc galaxies occupying the parameter space $\tau < 1.5$ Gyr is 29.4 per cent, and therefore suggest that quenching mechanisms with these time-scales are capable of destroying the disc-dominated nature of galaxies. This is most likely an overestimate of the mechanisms with time-scales that can cause a morphological change because of the observability of those galaxies which undergo such a rapid quench; Martin et al. (2007) showed that after considering the time spent in the green valley, the fraction of galaxies undergoing a rapid quench quadruples.

All of this evidence suggests that there are not just two routes for galaxies through the green valley as concluded by S14, but a continuum of quenching time-scales which we can divide into three general regimes: rapid ($\tau < 1.0$ Gyr), intermediate ($1.0 < \tau < 2.0$ Gyr) and slow ($\tau > 2.0$ Gyr). The intermediate-quenching time-scales reside in the space between the extremes sampled by the UV/optical diagrams of S14; the inclusion of the intermediate galaxies in this investigation (unlike in S14) and the more precise Bayesian analysis, quantifies this range of τ and specifically ties the intermediate time-scales to all variations of galaxy morphology.

4.4 Blue cloud galaxies

Since the blue cloud is considered to be primarily made of star-forming galaxies, we expect STARPY to have some difficulty in determining the most likely quenching model to describe them, as confirmed by Fig. 10. The attempt to characterize a star-forming galaxy with a quenched SFH model leads STARPY to attribute the extremely blue colours of the majority of these galaxies to fast quenching at recent times (i.e. very little change in the SFR; see the right-hand panel of Fig. 10 in comparison with the bottom panel of Fig. 4).

This is particularly apparent for the blue disc population. Perhaps even galaxies which are currently quenching slowly across the blue cloud cannot be well fitted by the quenching models implemented, as they still have high SFRs despite some quenching (although a galaxy has undergone quenching, star formation can still occur in a galaxy, just at a slower rate than at earlier times, described by τ).

There is a very small preference among blue bulge-dominated galaxies for slow quenching which began prior to $z \sim 0.5$. These

populations have been blue for a considerable period of time, slowly using up their gas for star formation by the Kennicutt–Schmidt law (Schmidt 1959; Kennicutt 1997). However, the major preference is for rapid quenching at recent times in the blue cloud; this therefore provides some support to the theories for blue ellipticals as either merger-driven (∼76 per cent; like those identified as recently quenched ellipticals with properties consistent with a merger origin by McIntosh et al. 2014) or gas inflow-driven reinvigorated star formation that is now slowly decreasing (∼24 per cent; such as the population of blue spheroidal galaxies studied by Kaviraj et al. 2013). However, we remind the reader that the quenching models used in this work do not provide an adequate fit to the blue cloud population.

The blue cloud is therefore primarily composed of both star-forming galaxies with any morphology and smooth galaxies which are undergoing a rapid quench, presumably after a previous event triggered star formation and turned them blue.

5 DISCUSSION

We have implemented a Bayesian statistical analysis of the SFHs of a large sample of galaxies morphologically classified by Galaxy Zoo. We have found differences between the SFHs of smooth- and disc-like galaxies across the CMD in the red sequence, green valley and blue cloud. In this section, we will speculate on the question: What are the possible mechanisms driving these differences?

5.1 Rapid-quenching mechanisms

Rapid quenching is much more prevalent in smooth galaxies than disc galaxies, and the red galaxies with NUV emission in this study are also much more likely to be characterized by a rapid-quenching model than green valley galaxies (ignoring blue cloud galaxies due to their apparent poor fit by the quenching models, see Fig. 10). In the green valley, there is also a distinct lack of preference for rapid-quenching time-scales with $\tau < 0.5$ Gyr; however, we must bear in mind the observability of a rapid-quenching history declines with decreasing τ. Rapid mechanisms may be more common in the green valley than seen in Fig. 9; however, this observability should not depend on morphology so we can still conclude that rapid-quenching mechanisms are detected more for smooth rather than disc galaxies. This suggests that this rapid-quenching mechanism causes a change in morphology from a disc- to a smooth-like galaxy as it quickly traverses the CMD to the red sequence, supported by the number of disc galaxies that would need to undergo a morphological change in order for the disc : smooth ratio of galaxies in the green valley to match that of the red galaxies (see Section 4.3). From this indirect evidence, we suggest that this rapid-quenching mechanism is due to major mergers.

Inspection of the galaxies contributing to this area of probability reveals that this does not arise due to *currently* merging pairs missed by GZ users which were therefore not excluded from the sample (see Section 2.2), but by typical smooth galaxies with red optical and NUV colours that the model attributes to rapid quenching at early times. Although a prescription for modelling a merger in the SFH is not included in this work, we can still detect the after effects (see Section 5.4 for future work planned with STARPY).

One simulation of interest by Springel, Di Matteo & Hernquist (2005) showed that feedback from black hole activity is a necessary component of destructive major mergers to produce such rapid-quenching time-scales. Powerful quasar outflows remove much of

the gas from the inner regions of the galaxy, terminating star formation on extremely short time-scales. Bell et al. (2006), using data from the COMBO-17 redshift survey ($0.4 < z < 0.8$), estimate a merger time-scale from being classified as a close galaxy pair to recognisably disturbed as ∼0.4 Gyr. Springel et al. (2005) consequently find using hydrodynamical simulations that after ∼1 Gyr the merger remnant has reddened to $u − r \sim 2.0$. This is in agreement with our simple quenching models which show (Fig. 7) that within ∼1 Gyr the models with an SFH with $\tau < 0.4$ Gyr have reached the red sequence with $u − r \gtrsim 2.2$. This could explain the preference for red disc galaxies with rapid-quenching time-scales (31.3 per cent), as they may have undergone a major merger recently but are still undergoing a morphological change from disc, to disturbed, to an eventual smooth galaxy (see also van der Wel et al. 2009).

We reiterate that this rapid-quenching mechanism occurs much more rarely in green valley galaxies of both morphologies than for the subset of red sequence galaxies studied, however, does not fully characterize all the galaxies in either the red sequence or green valley. Dry major mergers therefore do not fully account for the formation of any galaxy type at any redshift, supporting the observational conclusions made by Bell et al. (2007), Bundy, Treu & Ellis (2007), Kaviraj (2014b) and simulations by Genel et al. (2008).

5.2 Intermediate-quenching mechanisms

Intermediate-quenching time-scales are found to be equally prevalent across populations for both smooth and disc galaxies across cosmic time, particularly in the green valley. Intermediate time-scales are the prevalent mechanism for quenching smooth green valley galaxies, unlike the rapid-quenching prevalent for red galaxies. We suggest that this intermediate-quenching route must therefore be possible with routes that both preserve and transform morphology. It is this result of another route through the green valley that is in contradiction with the findings of S14.

If we once again consider the simulations of Springel et al. (2005), this time without any feedback from black holes, they suggest that if even a small fraction of gas is not consumed in the starburst following a merger (either because the mass ratio is not large enough or from the lack of strong black hole activity) the remnant can sustain star formation for periods of several gigayears. The remnants from these simulations take ∼5.5 Gyr to reach red optical colours of $u − r \sim 2.1$. We can see from Fig. 7 that the models with intermediate-quenching time-scales of $1.0 \lesssim \tau$ [Gyr] $\lesssim 2.0$ take approximately 2.5−5.5 Gyr to reach these red colours.

We speculate that the intermediate-quenching time-scales are caused by gas rich major mergers, major mergers without black hole feedback and from minor mergers, the latter of which is the dominant mechanism. This is supported by the findings of Lotz et al. (2008) who find that the detectability time-scales for equal-mass gas-rich mergers with large initial separations range from ∼1.1−1.9 Gyr, and of Lotz et al. (2011), who find in further simulations that as the baryonic gas fraction in a merger with mass ratios of 1:1–1:4 increases, so does the time-scale of the merger from ∼0.2 Gyr (with little gas, as above for major mergers causing rapid-quenching time-scales) up to ∼1.5 Gyr (with large gas fractions). Here, we are assuming that the morphologically detectable time-scale of a merger is roughly the same order as the quenching time-scale. However, we must consider the existence of a substantial population of blue ellipticals (Schawinski et al. 2009), which are thought to be post-merger systems with no detectable morphological signatures of a merger but with the merger-induced starburst

still detectable in the photometry. This photometry is an indicator for the SFH and therefore should present with longer time-scales for the photometric effects of a merger than found in the simulations by Lotz et al. (2008, 2011). Observing this link between the time-scale for the morphological observability of a merger and the time-scales for the star formation induced by a merger is problematic, as evidenced by the lack of literature on the subject.

Lotz et al. (2008) also show that the remnants of these simulated equal-mass gas-rich disc mergers (wet disc mergers) are observable for $\gtrsim 1$ Gyr post-merger and state that they appear 'disc-like and dusty' in the simulations, which is consistent with an 'early-type spiral morphology'. Such galaxies are often observed to have spiral features with a dominant bulge, suggesting that such galaxies may divide the votes of the GZ2 users, producing vote fractions of $p_s \sim p_d \sim 0.5$. We believe this is why the intermediate-quenching time-scales are equally dominant for both smooth and disc galaxies across each population in Figs 8 and 9.

Other simulations (e.g. such as Robertson et al. 2006 and Barnes 2002) support the conclusion that both gas-rich major mergers and minor mergers can produce disc-like remnants. Observationally, Darg et al. (2010) showed an increase in the spiral to elliptical ratio for merging galaxies ($0.005 < z < 0.1$) by a factor of 2 compared to the general population. They attribute this to the much longer time-scales during which mergers of spirals are observable compared to mergers with elliptical galaxies, confirming our hypothesis that the quenching time-scales $\tau < 1.5$ Gyr preferred by disc galaxies may be undergoing mergers which will eventually lead to a morphological change. Similarly, Casteels et al. (2013) observe that galaxies ($0.01 < z < 0.09$) which are interacting often retain their spiral structures and that a spiral galaxy which has been classified as having 'loose winding arms' by the GZ2 users are often entering the early stages of mergers and interactions.

40.6 per cent of the probability for smooth galaxies in the green valley arises due to intermediate-quenching time-scales (see Fig. 9); this is in agreement with work done by Kaviraj (2014a, 2014b) who by studying SDSS photometry ($z < 0.07$) state that approximately half of the star formation in galaxies is driven by minor mergers at $0.5 < z < 0.7$ therefore exhausting available gas for star formation and consequently causing a gradual decline in the SFR. This supports earlier work by Kaviraj et al. (2011) who, using multiwavelength photometry of galaxies in COSMOS (Scoville et al. 2007), found that 70 per cent of early-type galaxies appear morphologically disturbed, suggesting either a minor or major merger in their history. This is in agreement with the total percentage of probability with $\tau < 2.0$ [Gyr]; 73.9 and 59.3 per cent, for the smooth red and green galaxies in Figs 8 and 9, respectively. Note that the star formation model used here is a basic one and has no prescription for reignition of star formation post-quench which can also cause morphological disturbance of a galaxy, like those detected by Kaviraj et al. (2011).

Darg et al. (2010) show in their fig. 6 that that beyond a merger ratio of 1: 10 (up to ~1: 100), green is the dominant average galaxy colour of the visually identified merging pair in GZ. These mergers are also dominated by spiral–spiral mergers as opposed to elliptical–elliptical and elliptical–spiral. This supports our hypothesis that these intermediate time-scales dominating in the green valley are caused in part by minor mergers. This is contradictory to the findings of Mendez et al. (2011) who find the merger fraction in the green valley is much lower than in the blue cloud; however, they use an analytical light decomposition indicator (Gini/M_{20}; see Lotz et al. 2008) to identify their mergers, which tend to detect major mergers more easily than minor mergers. We have discussed the

lower likelihood of a green valley galaxy to undergo a rapid quench, which we have attributed to major mergers (see Section 5.1), despite the caveat of the observability and believe that this may have been the phenomenon that Mendez et al. (2011) detected.

The resultant intermediate-quenching time-scales occur due to one interaction mechanism, unlike the rapid quenching, which occurs due to a major merger combined with AGN feedback, and decreases the SFR over a short period of time. Therefore, any external event which can cause either a burst of star formation (depleting the gas available) or directly strip a galaxy of its gas, for example galaxy harassment, interactions, ram pressure stripping, strangulation and interactions internal to clusters, would cause quenching on an intermediate time-scale. Such mechanisms would be the dominant cause of quenching in dense environments; considering that the majority of galaxies reside in groups or clusters (Coil et al. 2008 find that green valley galaxies are just as clustered as red sequence galaxies), it is not surprising that the majority of our galaxies are considered intermediate in morphology (see Table 1) and therefore are undergoing or have undergone such an interaction.

5.3 Slow-quenching time-scales

Although intermediate- and rapid-quenching time-scales are the dominant mechanisms across the CMD, together they cannot completely account for the quenching of disc galaxies. S14 concluded that slow-quenching time-scales were the most dominant mechanism for disc galaxies. However, we show that (i) intermediate-quenching time-scales are equally important in the green valley and (ii) rapid-quenching time-scales are equally important for red galaxies with NUV emission. There is also a significantly lower preference for smooth galaxies to undergo such slow-quenching time-scales, suggesting that the evolution (or indeed creation) of typical smooth galaxies is dominated by processes external to the galaxy. This is excepting galaxies in the blue cloud where a small amount of slow evolution of blue ellipticals is occurring, presumably after a reinvigoration of star formation which is slowly depleting the gas available according to the Kennicutt–Schmidt law.

Bamford et al. (2009) using GZ1 vote fractions of galaxies in the SDSS, found a significant fraction of high stellar mass red spiral galaxies in the field. As these galaxies are isolated from the effects of interactions from other galaxies, the slow-quenching mechanisms present in their preferred SFHs are most likely due to secular processes (i.e. mechanisms internal to the galaxy, in the absence of sudden accretion or merger events; Kormendy & Kennicutt 2004; Sheth et al. 2012). Bar formation in a disc galaxy is such a mechanism, whereby gas is funnelled to the centre of the galaxy by the bar over long time-scales where it is used for star formation (Masters et al. 2012; Saintonge et al. 2012; Cheung et al. 2013), consequently forming a 'pseudo-bulge' (Kormendy et al. 2010; Simmons et al. 2013).

If we believe that these slow-quenching time-scales are due to secular evolution processes, this is to be expected since these processes do not change the disc-dominated nature of a galaxy.

5.4 Future work

Due to the flexibility of our model, we believe that the STARPY module will have a significant number of future applications, including the investigation of various different SFHs (e.g. constant SFR and starbursts). Considering the number of magnitude bands available across the SDSS, further analysis will also be possible with a larger set of optical and NUV colours, providing further constraints and

to ensure a more complete sample, containing a larger fraction of typical red sequence galaxies, if the need for NUV photometry was replaced with another band. It would also be of interest to consider galaxies at higher redshift (e.g. out to $z \sim 1$ with *Hubble Space Telescope* photometry and the GZ:Hubble project, see Melvin et al. 2014 for first results) and consider different redshift bins in order to study the build-up of the red sequence with cosmic time.

With further use of the robust, detailed GZ2 classifications, we believe that STARPY will be able to distinguish any statistical difference in the SFHs of barred versus non-barred galaxies. This will require a simple swap of $\{p_s, p_d\}$ with $\{p_{bar}, p_{nobar}\}$ from the available GZ2 vote fractions. We believe that this will aid in the discussion of whether bars act to quench star formation (by funnelling gas into the galaxy centre) or promote star formation (by causing an increase in gas density as it travels through the disc) both sides of which have been fiercely argued (Sheth et al. 2005; Ellison et al. 2011; Masters et al. 2011, 2012).

Further application of the STARPY code could be to investigate the SFH parameters of:

(i) currently merging/interacting pairs in comparison to those galaxies classified as merger remnants, from their degree of morphological disturbance,

(ii) slow rotators and fast rotators which are thought to result from dry major mergers on the red sequence (Emsellem et al. 2011) and gas rich, wet major mergers (Emsellem et al. 2007), respectively,

(iii) field and cluster galaxies using the projected neighbour density, Σ, from Baldry et al. (2006).

6 CONCLUSION

We have used morphological classifications from the GZ2 project to determine the morphology-dependent SFHs of galaxies via a Bayesian analysis of an exponentially declining star formation quenching model. We determined the most likely parameters for the quenching onset time, t_q and quenching time-scale τ in this model for galaxies across the blue cloud, green valley and red sequence to trace galactic evolution across the CMD. We find that the green valley is indeed a transitional population for all morphological types (in agreement with S14); however, this transition proceeds slowly for the majority of disc-like galaxies and occurs rapidly for the majority of smooth-like galaxies in the red sequence. However, in addition to S14, our Bayesian approach has revealed a more nuanced result, specifically that the prevailing mechanism across all morphologies and populations is quenching with intermediate time-scales. Our main findings are as follows.

(i) The subset of red sequence galaxies with NUV emission studied in this investigation are found to have similar preferences for quenching time-scales compared to the green valley galaxies, but occurs at earlier quenching times regardless of morphology (see Figs 8 and 9). Therefore, the quenching mechanisms currently occurring in the green valley were also active in creating the 'blue end of the red sequence' at earlier times, confirming that the green valley is indeed a transitional population, regardless of morphology.

(ii) We confirm that the typical red galaxy with NUV emission studied in this investigation, is elliptical in morphology and conclude that it has undergone a rapid to intermediate quench at some point in cosmic time, resulting in a very low current SFR (see Section 4.2).

(iii) The green valley as it is currently observed is dominated by very slowly evolving disc-like galaxies along with intermediate- and smooth-like galaxies which pass across it with intermediate time-scales within $\sim 1.0-1.5$ Gyr (see Section 4.3).

(iv) There are many different time-scales responsible for quenching, causing a galaxy to progress through the green valley, which are dependent on galaxy type, with the smooth- and disc-like galaxies each having different dominant SFHs across the CMD. These time-scales can be roughly split into three main regimes: rapid ($\tau <$ 1.0Gyr), intermediate ($1.0 < \tau [Gyr] < 2.0$) and slow ($\tau > 2.0$ Gyr) quenching.

(v) Blue cloud galaxies are not well fitted by a quenching model of star formation due to the continuous high SFRs occurring (see Fig. 10).

(vi) Rapid-quenching time-scales are detected with a lower probability for green valley galaxies than the subset of red sequence galaxies studied. We speculate that this quenching mechanism is caused by major mergers with black hole feedback, which are able to expel the remaining gas not initially exhausted in the merger-induced starburst and which can cause a change in morphology from disc- to bulge dominated. The colour-change time-scales from previous simulations of such events agree with our derived time-scales (see Section 5.1). These rapid time-scales are instrumental in forming red galaxies; however, galaxies at the current epoch passing through the green valley do so at more intermediate time-scales (see Fig. 9).

(vii) Intermediate-quenching time-scales ($1.0 < \tau [Gyr] < 2.0$) are found with constant probability across red and green galaxies for both smooth- and disc-like morphologies, the time-scales for which agree with observed and simulated minor merger time-scales (see Section 5.2). We hypothesize such time-scales can be caused by a number of external processes, including gas-rich major mergers, mergers without black hole feedback, galaxy harassment, interactions and ram pressure stripping. The time-scales and observed morphologies from previous studies agree with our findings, including that this is the dominant mechanisms for intermediate galaxies such as early-type spiral galaxies with spiral features but a dominant bulge, which split the GZ2 vote fractions (see Section 5.2).

(viii) Slow-quenching time-scales are the most dominant mechanism in the disc galaxy populations across the CMD. Disc galaxies are often found in the field; therefore, we hypothesize that such slow-quenching time-scales are caused by secular evolution and processes internal to the galaxy (see Section 4.4). We also detect a small amount of slow-quenching time-scales for blue elliptical galaxies which we attribute to a reinvigoration of star formation, the peak of which has passed and has started to decline by slowly depleting the gas available (see Section 4.4).

(ix) Due to the flexibility of this model we believe that the STARPY module compiled for this investigation will have a significant number of future applications, including the different SFHs of barred versus non-barred galaxies, merging versus merger remnants, fast versus slow rotating elliptical galaxies and cluster versus field galaxies (see Section 5.4).

REFERENCES

Aihara H. et al., 2011, ApJS, 193, 29
Arnouts S. et al., 2007, A&A, 476, 137
Baldry I. K., Glazebrook K., Brinkmann J., Ivezić Ž., Lupton R. H., Nichol R. C., Szalay A. S., 2004, ApJ, 600, 681
Baldry I. K., Balogh M. L., Bower R. G., Glazebrook K., Nichol R. C., Bamford S. P., Budavari T., 2006, MNRAS, 373, 469
Ball N. M., Loveday J., Brunner R. J., 2008, MNRAS, 383, 907
Bamford S. P. et al., 2009, MNRAS, 393, 1324
Barnes J. E., 2002, MNRAS, 333, 481

Barro G. et al., 2013, ApJ, 765, 104
Bell E. F. et al., 2004, ApJ, 608, 752
Bell E. F., Phleps S., Somerville R. S., Wolf C., Borch A., Meisenheimer K., 2006, ApJ, 652, 270
Bell E. F., Zheng X. Z., Papovich C., Borch A., Wolf C., Meisenheimer K., 2007, ApJ, 663, 834
Béthermin M. et al., 2012, ApJ, 757, L23
Blanton M. R., Roweis S., 2007, AJ, 133, 734
Blanton M. R. et al., 2005, AJ, 129, 2562
Bower R. G., Lucey J. R., Ellis R. S., 1992, MNRAS, 254, 601
Brammer G. B. et al., 2009, ApJ, 706, 173
Brinchmann J., Charlot S., White S. D. M., Tremonti C., Kauffmann G., Heckman T., Brinkmann J., 2004, MNRAS, 351, 1151
Bruzual G., Charlot S., 2003, MNRAS, 344, 1000 (BC03)
Bundy K., Treu T., Ellis R. S., 2007, ApJ, 655, L5
Canalizo G., Stockon A., 2001, ApJ, 555, 719
Cardelli J. A., Clayton G. C., Mathis J. S., 1989, ApJ, 345, 245
Casteels K. et al., 2013, MNRAS, 429, 1051
Chabrier G., 2003, PASP, 115, 763
Chen X. Y., Liang Y. C., Hammer F., Prugniel Ph., Zhong G. H., Rodrigues M., Zhao Y. H., Flores H., 2010, A&A, 515, 101
Chester C., Roberts M. S., 1964, AJ, 69, 635
Cheung E. et al., 2012, ApJ, 760, 131
Cheung E. et al., 2013, ApJ, 779, 162
Coil A. L. et al., 2008, ApJ, 672, 153
Conroy C., Gunn J. E., White M., 2009, ApJ, 699, 486
Constantin A., Hoyle F., Vogeley M. S., 2008, ApJ, 673, 715
Daddi E. et al., 2007, ApJ, 670, 156
Darg D. et al., 2010, MNRAS, 401, 1552
de Lucia G., Tornatore L., Frenk C. S., Helmi A., Navarro J. F., White Simon D. M., 2014, MNRAS, 445, 970
Di Matteo T., Springel V., Hernquist L., 2005, Nature, 433, 604
Driver S. P. et al., 2006, MNRAS, 368, 414
Elbaz D. et al., 2007, A&A, 468, 33
Ellison S. L., Nair P., Patton D. R., Scudder J. M., Mendel J. T., Simard L., 2001, MNRAS, 416, 2182
Emsellem E. et al., 2007, in Combes F., Palouš J., eds, Proc. IAU Symp. 235. Galaxy Evolution Across the Hubble Time. Cambridge University Press, Cambridge, p. 39
Eminian C., Kauffmann G., Charlot S., Wild V., Bruzual G., Rettura A., Loveday J., 2008, MNRAS, 384, 930
Emsellem E. et al., 2011, MNRAS, 414, 888
Faber S. M. et al., 2007, ApJ, 665, 265
Falkenberg M. A., Kotulla R., Fritze U., 2009, MNRAS, 397, 1954
Fang J. J., Faber S. M., Koo D. C., Dekel A., 2013, ApJ, 776, 63
Foreman-Mackey D., Hogg D. W., Lang D., Goodman J., 2013, PASP, 125, 306
Genel S. et al., 2008, ApJ, 688, 789
Glazebrook K. et al., 2003, ApJ, 587, 55
González V., Labbé I., Bouwens R. J., Illingworth G., Franx M., Kriek M., Brammer G. B., 2010, ApJ, 713, 115
Gonçalves T. S., Martin D. C., Menéndez-Delmestre K., Wyder T. K., Koekemoer A., 2012, ApJ, 759, 67
Goodman J., Weare J., 2010, Commun. Appl. Math. Comput. Sci., 5, 65
Heinis S. et al., 2014, MNRAS, 437, 1268
Jarosik N. et al., 2011, ApJS, 192, 18
Kauffman G. et al., 2003, MNRAS, 341, 33
Kaviraj S., 2014a, MNRAS, 437, L41
Kaviraj S., 2014b, MNRAS, 440, 2944
Kaviraj S., Tan K.-M., Ellis R. S., Silk J., 2011, MNRAS, 411, 2148
Kaviraj S. et al., 2013, MNRAS, 428, 925
Kennicutt R. C., 1997, ApJ, 498, 491
Kormendy J., Kennicutt R. J., 2004, ARA&A, 42, 603
Kormendy J., Drory N., Bender R., Cornell M. E., 2010, ApJ, 723, 54
Kriek M. et al., 2010, ApJ, 722, L64
Lintott C. J. et al., 2008, MNRAS, 389, 1179
Lintott C. J. et al., 2011, MNRAS, 410, 166

Lotz J., Jonsson P., Cox T. J., Primack J. R., 2008, MNRAS, 391, 1137

Lotz J., Jonsson P., Cox T. J., Croton D., Primack J. R., Somerville R. S., Stewart K., 2011, MNRAS, 742, 103

MacKay D. J. C., 2003, Information Theory, Inference and Learning Algorithms. Cambridge Univ. Press, Cambridge

McIntosh D. H. et al., 2014, MNRAS, 442, 533

Marasco A., Fraternali F., Binney J. J., 2012, MNRAS, 419, 1107

Maraston C., 2005, MNRAS, 362, 799

Martin D. C. et al., 2005, ApJ, 619, L1

Martin D. C. et al., 2007, ApJS, 173, 342

Masters K. L. et al., 2010, MNRAS, 405, 783

Masters K. L. et al., 2011, MNRAS, 411, 2026

Masters K. L. et al., 2012, MNRAS, 424, 2180

Melbourne J. et al., 2012, ApJ, 748, 47

Melvin T. et al., 2014, MNRAS, 438, 2882

Mendez A. J., Coil A. L., Lotz J., Salim S., Moustakas J., Simard L., 2011, ApJ, 736, 110

Miller N. A., Rose J. A., Cecil G., 2011, ApJ, 727, L15

Nair P. B., Abraham R. G., 2010, ApJS, 186, 427

Nandra K. et al., 2007, ApJ, 660, L11

Noeske K. G. et al., 2007, ApJ, 660, L43

Oh K., Sarzi M., Schawinski K., Yi S. K., 2011, ApJS, 195, 13

Padmanabhan N. et al., 2008, ApJ, 674, 1217

Pan Z., Li J., Lin W., Wang J., Kong X., 2014, ApJ, 792, L4

Peng Y. et al., 2010, ApJ, 721, 193

Robertson B., Bullock J. S., Cox T. J., Di Matteo T., Hernquist L., Springel V., Yoshida N., 2006, ApJ, 645, 986

Robitaille T. P. et al., 2013, A&A, 558, A33

Saintonge A. et al., 2012, ApJ, 758, 73

Salim S. et al., 2007, ApJS, 173, 267

Sánchez-Blázquez P., Gorgas J., Cardiel N., González J. J., 2006, A&A, 457, 809

Schawinski K., Thomas D., Sarzi M., Maraston C., Kaviraj S., Joo S.-J., Yi S. K., Silk J., 2007, MNRAS, 382, 1415

Schawinski K. et al., 2009, MNRAS, 396, 818

Schawinski K. et al., 2014, MNRAS, 440, 889 (S14)

Schiminovich D. et al., 2007, ApJS, 173, 315

Schmidt M., 1959, ApJ, 129, 243

Scoville N. et al., 2007, ApJS, 172, 1

Sheth K., Vogel S. N., Regan M. W., Thornley M. D., Teuben P. J., 2005, ApJ, 632, 217

Sheth K., Melbourne J., Elmegreen D. M., Elmegreen B. G., Athanassoula E., Abraham R. G., Weiner B. J., 2012, ApJ, 758, 136

Simmons B. D. et al., 2013, MNRAS, 429, 2199

Sivia D. S., 1996, Data Analysis: A Bayesian Tutorial. Oxford Univ. Press, Oxford

Skibba R. A. et al., 2009, MNRAS, 399, 966

Springel V., Di Matteo T., Hernquist L., 2005, ApJ, 620, L79

Strateva I. et al., 2001, AJ, 122, 1861

Taylor M. B., 2005, in Shopbell P. L., Britton M. C., Ebert R., eds, ASP Conf. Ser. Vol. 347, Astronomical Data Analysis Software and Systems XIV. Astron. Soc. Pac., San Francisco, p. 29

Trager S. C., Faber S. M., Worthey G., González J. J., 2000, AJ, 120, 165

Tojero R., Heavens A. F., Jimenez R., Panter B., 2007, MNRAS, 381, 1252

Tojeiro R. et al., 2013, MNRAS, 432, 359

van der Wel A., Rix H.-W., Holden B. P., Bell E. F., Robaina A. R., 2009, ApJ, 706, L120

Vazdekis A., Sánchez-Blázquez P., Falcón-Barroso J., Cenarro A. J., Beasley M. A., Cardiel N., Gorgas J., Peletier R. F., 2010, MNRAS, 404, 1639

Willett K. et al., 2013, MNRAS, 435, 2835

Willmer C. N. A. et al., 2006, ApJ, 647, 853

Wong I. et al., 2012, MNRAS, 420, 1684

Wyder T. K. et al., 2007, ApJS, 173, 293

York D. G. et al., 2000, AJ, 120, 1579

APPENDIX A: TESTING STARPY

In order to test that STARPY can find the correct quenching model for a given observed colour, 25 synthesized galaxies were created with known SFHs (i.e. known values of θ) from which optical and NUV colours were generated. These were input into STARPY to ensure that the known values of θ were reproduced, within error, for each of the 25 synthesized galaxies. Fig. A1 shows the results for each of these 25 synthesized galaxies, with the known values of θ shown by the red lines. In some cases, this red line does not coincide with the peak of the distribution shown in the histograms for one parameter; however, in all cases the intersection of the red lines is within the sample contours.

We find pepeaks in the histograms across all areas of the parameter space in both dimensions of $[t, \tau]$, this ensures that the results presented in Figs 8–10 arise due to a superposition of extended probability distributions, as opposed to a bimodal distribution of probability distributions across all galaxies.

APPENDIX B: USING LOOK-UP TABLES

Considering the size of the sample in this investigation of 126 316 galaxies total, a three-dimensional look-up table (in observed time, quenching time and quenching rate) was generated using the SFH function in STARPY to speed up the run time. Fig. B1 shows an example of how using the look-up table in place of the full function does not affect the results to a significant level. Table B1 quotes the median walker positions (the 50th percentile of the Bayesian probability distribution) along with their $\pm 1\sigma$ ranges for both methods in comparison to the true values specified to test STARPY. The uncertainties incorporated into the quoted values by using the look-up table are therefore minimal with a maximum $\Delta = 0.043$.

APPENDIX C: DISCARDING POORLY FITTED GALAXIES

We discard walker positions returned by STARPY with a corresponding probability of $P(\theta_k|d_k) < 0.2$ in order to exclude galaxies which are not well fitted by the quenching model; for example blue cloud galaxies which are still star forming will be poorly fit by a quenching model (see Section 3.1). This raises the issue of whether we exclude a significant fraction of our galaxy sample and whether those galaxies reside in a specific location of the colour–magnitude. The fraction of galaxies which had all or more than half of their walker positions discarded due to low probability are shown in Table C1.

This is not a significant fraction of either population, therefore this shows that the STARPY module is effective in fitting the majority of galaxies and that this method of discarding walker positions ensures that poorly fitted galaxies are removed from the analysis of the results. Fig. C1 shows that these galaxies with discarded walker positions are also scattered across the optical–NUV colour–colour diagram, and therefore, STARPY is also effective in fitting galaxies across this entire plane.
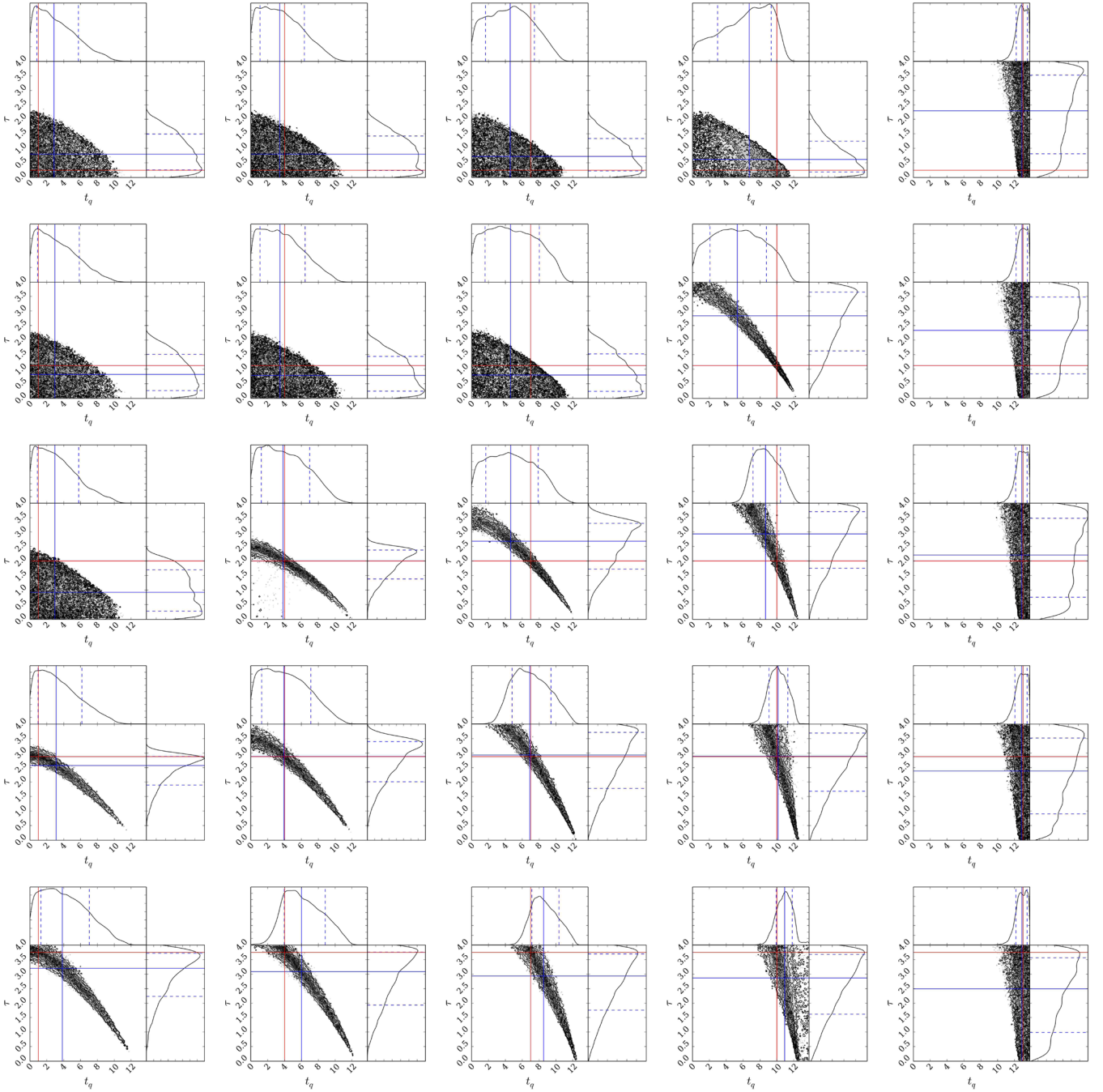
Figure A1. Results from STARPY for an array of synthesized galaxies with known, i.e. *true*, t_q and τ values (marked by the red lines) using the complete function to calculate the predicted colour of a proposed set of θ values in each MCMC iteration, assuming an error on the calculated known colours of $\sigma_{u-r} = 0.124$ and $\sigma_{NUV-u} = 0.215$, the average errors on the GZ sample colours. In each case STARPY succeeds in locating the true parameter values within the degeneracies of the SFH model. These degeneracies can clearly be seen in Fig. 4.

APPENDIX D: OBSERVABILITY OF QUENCHING GALAXIES

The numbers of galaxies found undergoing a rapid quench will be underestimated compared to the true value due to their observabil-ity, i.e. their time spent in the green valley is extremely short, so detecting a galaxy there is difficult. We considered this time spent in the green valley across our model parameter space of SFHs and the results are shown below in Fig. D1.
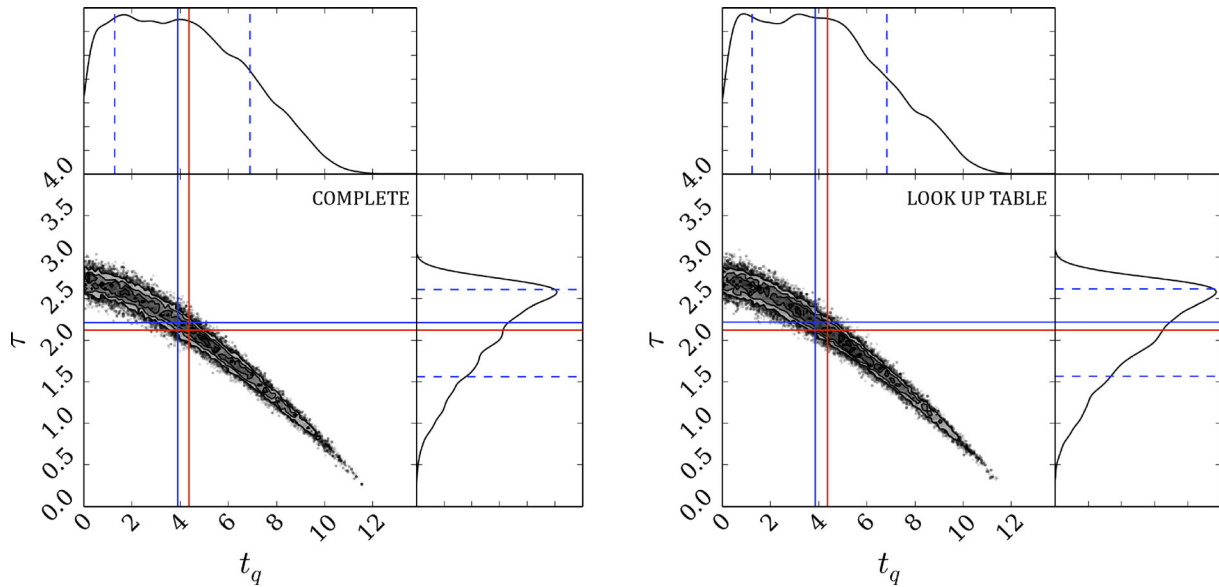
Figure B1. Left-hand panel: results from STARPY for true t_q and τ values (red lines) using the complete function to calculate the predicted colour of a proposed set of θ values in each MCMC iteration. The median walker position (the 50th percentile of the Bayesian probability distribution) is shown by the solid blue line with the dashed lines encompassing 68 per cent ($\pm 1\sigma$) of the samples (the 16th and 84th percentile positions). The time taken to run for a single galaxy using this method is approximately 2 h. Right-hand panel: results from STARPY for true t_q and τ values using a look-up table generated from the complete function to calculate the predicted colour of a proposed set of θ values in each MCMC iteration. The time taken to run for a single galaxy using this method is approximately 2 min.

Table B1. Median walker positions (the 50th percentile; as shown by the blue solid lines in Fig. B1) found by STARPY for a single galaxy, using the complete SFH function and a look-up table to speed up the run time. The errors quoted define the region in which 68 per cent of the samples are located, shown by the dashed blue lines in Fig. B1. The known true values are also quoted, as shown by the red lines in Fig. B1. All values are quoted to three significant figures.

	t_q	τ
True	4.37	2.12
Complete	$3.893 \pm^{3.014}_{2.622}$	$2.215 \pm^{0.395}_{0.652}$
Look-up table	$3.850 \pm^{2.988}_{2.619}$	$2.218 \pm^{0.399}_{0.649}$

Table C1. Number of galaxies in each population which had walker positions discarded due to low probability in order to exclude those galaxies from the analysis which were poorly fitted by this quenching model.

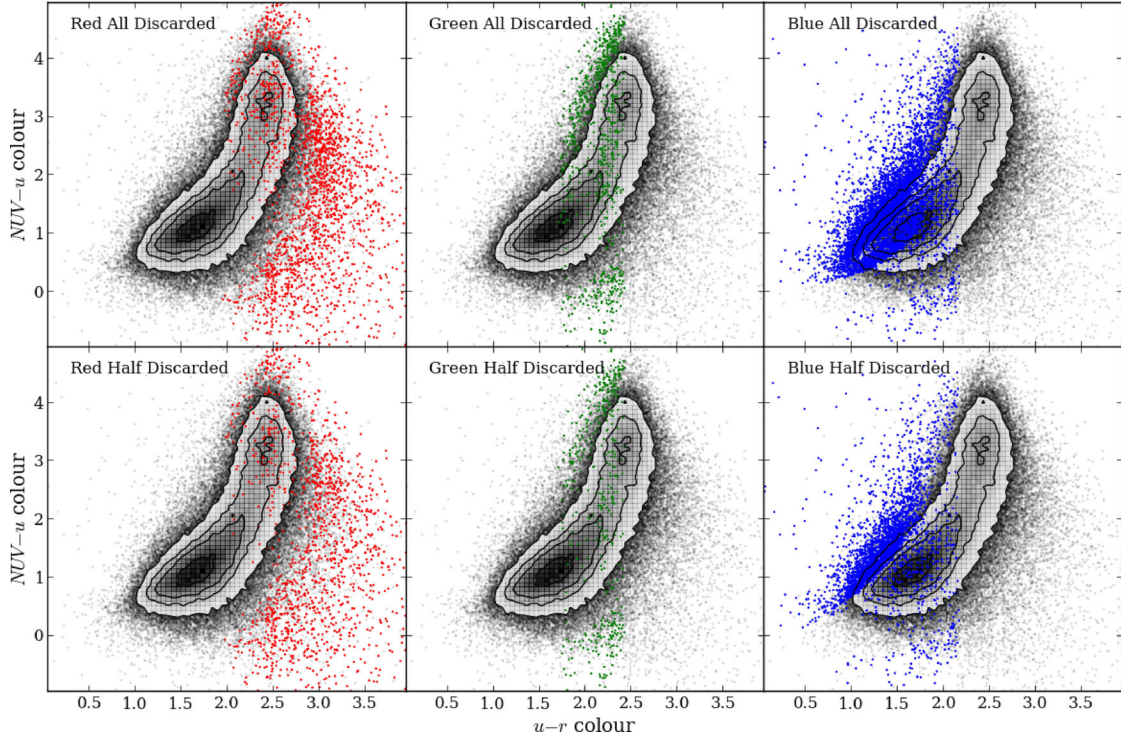|	Red sequence	Green valley	Blue cloud
All walkers discarded	1420	437	3109
	(7.00 per cent)	(2.41 per cent)	(5.37 per cent)
More than half walker positions discarded	2010	779	6669
	(9.92 per cent)	(4.30 per cent)	(11.52 per cent)

Figure C1. Contours show the full GZ2 sub-sample optical–NUV colour–colour diagram. The points show the positions of the galaxies which had all (top panels) or more than half (bottom panel) of their walker positions discarded due to their low probability for the red sequence (left), green valley (middle) and blue cloud (right).
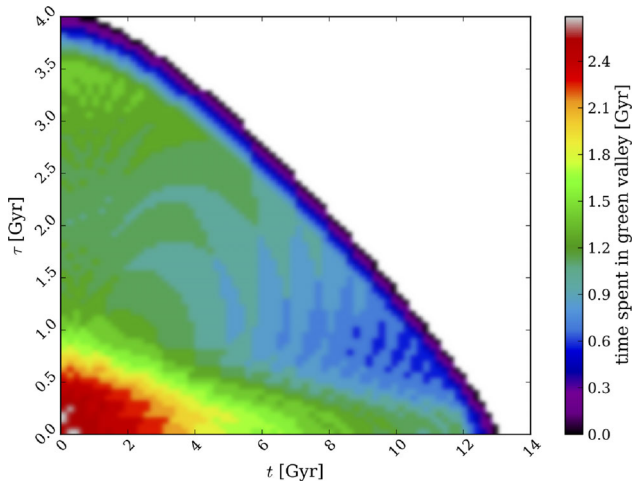

Figure D1. Plot showing the time spent in the green valley across the model SFH parameter space. This affects the observability of those galaxies which have quenched rapidly and recently and have passed too quickly through the green valley to be detected. The white region denotes those models with colours that do not enter the green valley by the present cosmic time.

This paper has been typeset from a TEX/LATEX file prepared by the author.